



JIMMA UNIVERSITY

JIMMA INSTITUTE OF TECHNOLOGY

SCHOOL OF GRADUATE STUDIES

FACULTY OF MATERIALS SCIENCE AND ENGINEERING

CHAIR OF MATERIALS SCIENCE AND ENGINEERING

MASTERS OF SCIENCE PROGRAM IN MATERIALS  
SCIENCE AND ENGINEERING

**“Computational study of the effects of Sr-dopant on  
the lattice thermal conductivity of  $Mg_2Si$   
thermoelectric material”**

By

Dita Deme Degefa(B.Sc.)

A Research Thesis Submitted to School of Graduate Studies of Jimma  
University in Partial Fulfillment of the Requirements of Masters of Science  
Degree in Materials science and Engineering

July 2021

Jimma, Ethiopia

JIMMA UNIVERSITY  
JIMMA INSTITUTE OF TECHNOLOGY  
SCHOOL OF GRADUATE STUDIES  
FACULTY OF MATERIALS SCIENCE AND ENGINEERING  
CHAIR OF MATERIALS SCIENCE AND ENGINEERING  
MASTERS OF SCIENCE PROGRAM IN MATERIALS  
SCIENCE AND ENGINEERING

**”Computational study of the effects of Sr-dopant on  
the lattice thermal conductivity of Mg<sub>2</sub>Si  
thermoelectric material”**

By

**Dita Deme Degefa (B.Sc.)**

A Research Thesis Submitted to School of Graduate Studies of Jimma University in Partial Fulfillment of the Requirements of Masters of Science Degree in Materials science and Engineering

Advisor: Dr. Mulualem Abebe (Ph.D)

Co-advisor: Dr. Sintayehu Mokonnen (Ph.D)

July 2021

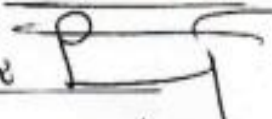

Jimma, Ethiopia

**JIMMA INSTITUTE OF TECHNOLOGY**  
**SCHOOL OF POST GRADUATE STUDIES**  
**FACULTY MATERIALS SCIENCE AND ENGINEERING**

**Computational study of the effects of Sr-dopant on the Lattice thermal conductivity  
of Mg<sub>2</sub>Si thermoelectric materials**

By  
**Dita Deme Degefa**

**APPROVED BY BOARD OF EXAMINERS**

1. <u>Dr. Paulos Tadesse</u>		<u>13 / 07 / 2021</u>
External Examiner	Signature	Date
2. <u>Dr. Olu Femi</u>		<u>13 / 07 / 2021</u>
Internal Examiner	Signature	Date
3. <u>Dr. Himanshu Rajan</u>		<u>13 / 07 / 2021</u>
Chairman of Examiner	Signature	Date
4. <u>Dr. Mulalem Abebe</u>		<u>13 / 07 / 2021</u>
Main Advisor	Signature	Date
5. <u>Dr. Sinau M</u>		<u>13 / 07 / 2021</u>
Co- Advisor	Signature	Date

## Declaration

This thesis, Computational study of the effects of Sr-dopant on the Lattice thermal conductivity of  $Mg_2Si$  thermoelectric material, is submitted in candidacy for partial fulfillment of M.Sc. degree in Materials Science and Engineering from Jimma Institute of Technology. Dita Deme at the School of Materials Science and Engineering has carried out this research work under the supervision of Dr. Muluaem Abebe and Dr. Sintayehu Mokonnen. The appropriateness of this thesis and its feasibility are believed to right and acknowledged by both the advisors and the advisee.

**Advisee: Mr.Dita Deme**

---

**Advisor: Dr. Muluaem Abebe**

---

**Co-adviser: Dr. Sintayehu Mokonnen**

---

## **Acknowledgment**

First of all, I would like to thank my advisors Dr. Muluaem Abebe (Asst. Prof.) and Dr. Sintayehu Mokonnen(Asst. prof.) for their motivation and supportive guidance, right from the moments of the selection of study area to the end of this thesis. Their eagerness and support have always inspired me to get many ideas to had launched and have finished this work. Without the support of countless colleagues, friends, and family, both personally and professionally, none of this would have been possible. I'm grateful for having had excellent collaborators especially Mr. Dereje Bekela, who had guided me in the training of computational simulations and software installation by fulfilling every necessary readable material, and Mr. Solomon Demise who had supported me with the basic scientific view of data analysis and documentations. Finally, I would like to thank the Jimma Institute of Technology(JIT), who had supported me financially, and the Department of materials science and engineering, which have been initially supporting me to get the chance of this a master's scholar.

## Abstract

*Due to its high abundance, low density, non-toxic nature, and low cost of production, Magnesium Silicide is very important for thermoelectric applications. In recent years enormous investigations have been done to improve the thermoelectric figure of merit (ZT) of Mg<sub>2</sub>Si-based thermoelectric (TE) material by both experimental and computational methods. In this study, the first-principles pseudopotentials based on density functional theory (DFT) had been applied to study the effect of Sr dopant on the lattice thermal conductivity of Mg<sub>2</sub>Si. The effects of Sr dopant on other properties like electronic structure, the density of state (DOS), and phonon properties of doped Mg<sub>2</sub>Si had also investigated. The lattice constant, Converged kinetic energy cutoff, and K-point grid had been optimized from Self-calculation field (SCF) calculations by quantum espresso software and CASTEP(Cambridge Serial Total Energy Package) code in Material studio software. After optimizations had been done, all other calculations related to the thermoelectric like Seebeck coefficient, electrical conductivity, and thermal conductivity had calculated within various temperature ranges from 20K to 800K for both native and doped Mg<sub>2</sub>Si. Finally, we acquired a very good result from Sr-doped (Mg<sub>16-x</sub>Si<sub>8</sub>Sr<sub>x</sub>, where 'x' is the amount of dopant atom). The lattice thermal conductivity had highly minimized to (0.02) W/Km at the temperature of (800) K for x =2 (Mg<sub>14</sub>Si<sub>8</sub>Sr<sub>2</sub>). It has shown a huge change when we compared to un-doped Mg<sub>16</sub>Si<sub>8</sub> in temperature ranges of (200-1000) K.*

**Key terms:** *Figure of merit, pseudopotentials, Density Functional Theory, Magnesium Silicide, Seebeck coefficient, Lattice thermal conductivity, phonon, BoltzTrap*

# Tables of contents

Declaration .....	i
Acknowledgment .....	ii
Abstract .....	iii
Tables of contents .....	iv
List of figure .....	vi
List of Acronym.....	vii
1. INTRODUCTION .....	1
1.1. Theoretical backgrounds .....	2
1.1.1. Thermoelectric effects and Performance of Thermoelectric Materials .....	2
1.1.2. Mg <sub>2</sub> Si based thermoelectric materials and their properties .....	4
1.2. Theoretical simulation.....	5
1.2.1. Density functional theory.....	5
1.2.2. Approximating the exchange-correlation energy.....	6
1.2.3. Electronic structure calculation.....	7
1.2.5. K-Points .....	9
1.2.6. Electronic transport properties .....	10
1.2.7. Phonon calculations .....	12
1.3. Statements of problem.....	15
1.4. Scopes.....	15
1.5. Objective .....	16
1.1.2. Specific objectives .....	16
2. LITERATURE REVIEWS .....	17

2.1	Introduction .....	17
2.2	Theoretical Review for Enhancing Thermoelectric Materials .....	18
2.2.1	Enhancing ZT in bulk materials.....	18
2.2.2	Novel approach.....	18
2.2.3	Mass fluctuation technique (Half Heusler Materials).....	19
2.2.4	Nanostructured thermoelectric.....	19
3.	COMPUTATIONAL METHODS.....	21
4.	RESULT AND DISCUSSION .....	24
4.1	Optimization and stability of crystal structures.....	24
4.2	Electronic properties Analysis .....	26
4.3	Phonon properties analysis .....	34
5.	CONCLUSION AND RECOMMENDATIONS .....	41
	APPENDIX B.....	44
	REFERENCES .....	48



## List of figure

Figure 1.1 A schematic representation of TE for charge carrier (a p- or an n-type material) .....	2
Figure 1.2 Crystal structures of Mg <sub>2</sub> Si(ant-fluorite structure) ([23] ).....	5
Figure 1.3 Electronic band structure of Mg <sub>2</sub> Si under compressive strain ([35]) .....	11
Figure 4.1 Geometry optimization.....	25
Figure 4.2 Bandstructure and DOS.....	27
Figure 4.3 Seebeck coefficients as a function of temperature and chemical potentials .....	28
Figure 4.4 Electrical conductivity as a function of temperature and chemical potentials .....	29
Figure 4.5 Electronic thermal conductivity as a function of T and chemical potentials .....	30
Figure 4.6 Electronic thermal conductivity per-relaxation time.....	31
Figure 4.7 Electrical conductivity as a function of temperature and the number of carriers.....	32
Figure 4.8 Seebeck coefficient as a function of temperature and the number of carriers.....	34
Figure 4.9 Power factor per relaxation time for the three compound.....	34
Figure 4.10 Thermodynamic properties of Mg <sub>2</sub> Si .....	35
Figure 4.11 Lattice thermal conductivity.....	38
Figure 4.12 The ratio of lattice thermal conductivity to electronic thermal conductivity .....	39

## List of Acronym

Boltzmann transport equation.....	BTE
Brillouin Zone .....	BZ
Carrier concentration .....	n
Density functional theory.....	DFT
The density of State.....	DOS
Electronic thermal conductivity.....	$k_e$
Electrical conductivity.....	K
exchange–correlation .....	(XC)
Face centered cubic .....	FCC
The figure of merit.....	ZT
Generalized Gradient Approximation.....	GGA
Hartree–Fock.....	(HF)
Harte-Fock exchange-correlation .....	Ex HF
Hexagonal close-packed .....	HCP
Kohn–Sham density functional theory .....	KS-DFT
Lattice thermal conductivity.....	$k_l$
Local density approximation.....	LDA
Lorenz number.....	L
Magnesium Silicide .....	Mg <sub>2</sub> Si
Nuclear Magnetic Resonance.....	NMR

Partial local density of states.....	PDOS
Perdew-Burke-Ernzerhof.....	PBE
Peierls–Boltzmann transport.....	PBTE
Phonon-glass electron crystal .....	PGEC
Power factor.....	PF
Seebeck coefficient.....	S
Self-calculation field .....	SCF
Self-interaction error .....	SIE
Strontium .....	Sr
Temperature difference.....	$\Delta T$
Thermoelectric effect.....	TE
Ultrasoft pseudopotentials.....	USP
Uniform electron gas.....	UEG

# 1. INTRODUCTION

The current issues over future energy consumption and the impact of fossil fuels on the environment have initiated the plan to seek alternative energy sources. Consequently, there is a need for new sources of energy other than fossil fuels [1, 2]. In addition to new energy sources, energy conversion technologies are also needed. Because most of the energy produced is lost as heat in industrial environments and our daily life, and conversion of these large amounts of the lost heat energy cannot be properly done and is inevitably wasted in the environment [3]. Consequently, the invention of the thermoelectric effect, which converts directly heat to electricity by TE materials or vice versa is the one promising solution is [4, 5]. Due to their ability to directly converting heat into electricity, Thermoelectric (TE) materials have been attracting intensive attention and can play an important role in improving waste energy harvesting efficiency [6-8].

The current global energy crisis will have resolved by thermoelectric materials that recover waste heat and transform it into electricity or vice versa. The climate change resulting from global warming is also reduced by TE materials which create opportunities for the development of energy harvesting, smart sensors, and the new concept of automobiles, thermo power wave sources, woodstoves, and diesel power plants [9]. Even though the applications of thermoelectric materials are wide by enhancing their properties, it has mainly been used in small areas such as refrigerators, a cooling device for laser diodes, and cooling seats in automobiles because of its efficiency. In this work, the theoretical background of thermoelectric materials based on  $Mg_2Si$  and related materials was briefly described in the following sections. The properties of undoped and doped  $Mg_2Si$  were deeply studied by materials modeling and simulation techniques. First-principles calculation, based on the DFT method was implemented for optimization, properties calculation, and evaluation of data. Boltzmann electrons transport properties evaluation was used for electronic properties calculation like Seebeck coefficient, electrical conductivity, and electronic thermal conductivity, while phonopy and phono3py were used to evaluate the phonon properties like thermodynamic properties, specific heat capacity group velocity, and lattice thermal conductivity respectively. In addition CASTEP code, one of the Materials studio 2017

packages, was used for calculations of bandstructure, the density of states, and some phonon properties of our material.

## 1.1. Theoretical backgrounds

### 1.1.1. Thermoelectric effects and Performance of Thermoelectric Materials

The TE effect or “Seebeck effect” is the direct conversion of a temperature difference to an electrical voltage of the two dissimilar electrical conductors or semiconductors. This can happen when the two sides of materials are exposed to different temperatures and consequently generate voltages across the two sides of the materials [3, 9]. Conversely, the generation of a temperature difference by applying a voltage to the system is called the “Peltier effect”. So, thermoelectric materials are fundamentally focused on these two phenomena by which temperature differences create electricity or application of voltage creates temperature differences [10]. At the atomic scale, when a temperature gradient is applied at both end sides of a thermocouple, the electrons and holes have a lower density at the hotter side and move faster, resulting in diffusion of electrons/ holes toward the cold side[4]. As a result, the potential difference is created at the two end side of the materials and generate an electric field across the system [11].

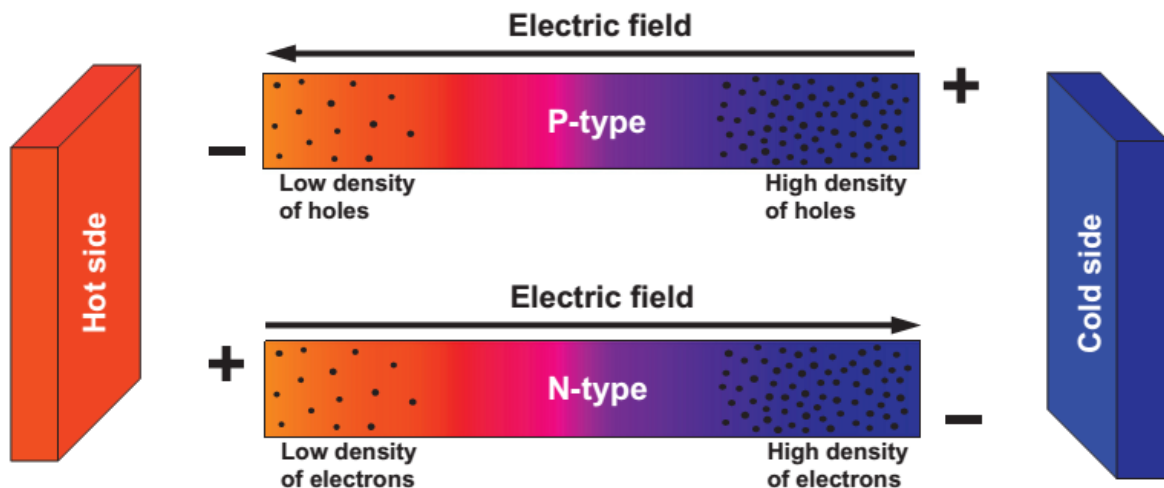


Figure 1.1 A schematic representation of TE for charge carrier (a p- or an n-type material) ( Lazaros Tzounis reviews; BoD – Books on Demand, 2019 M10 30 - 140 pages)

### 1.1.1.1. Seebeck coefficient

The voltage generated by thermoelectric effects is equal to  $S \times \Delta T$  where 'S' is Seebeck coefficient and  $\Delta T$  is temperature difference

$$S = \frac{\Delta V}{\Delta T} \quad (1)$$

An intrinsic property of the Seebeck coefficient is related to the electronic properties, which have a positive value for p-type and a negative value for n-type semiconductors. Seebeck coefficient is fatherly determining the power factor (PF) combined with electrical conductivity which is given by

$$PF = S^2 \sigma \quad (2)$$

Where ' $\sigma$ ' is electrical conductivity

### 1.1.1.2. Thermoelectric materials Figure of merit ZT

The figure of merit (ZT) is a dimensionless quantity in which the performances of thermoelectric materials and given by

$$ZT = \frac{S^2 \sigma T}{k} \quad (3)$$

Where 'T' and 'k' are absolute temperatures and thermal conductivities ( $k=k_e + k_l$ ). Thermal conductivity has resulted from electronic transport and lattice vibration or phonon vibration [11-13]. Maximizing the power factor  $S^2 \sigma$  and minimizing  $\kappa$  achieves a high ZT value. However, the interdependence between these transports coefficients makes optimization a challenging task. The complexity of optimizing both quantities leads the researchers to decay until a great reduction of thermal conductivity was both theoretically and experimentally proven in nanomaterials [14]. Since the electrical and thermal conductivities are interdependent through carrier concentration, optimizing one parameter will negatively affect the other parameter. Thus designing high-performance TE materials is difficult and the development of TE materials delays for many years [15, 16].

The appropriate solutions that overcome these difficulties are the proper approximation of these parameters. This can be approximated by maximizing the values of the parameter that has a positive effect (Seebeck coefficient, electrical conductivity) and minimizing the values of parameters that have a negative effect (thermal conductivity) [1] by improving the properties of TE materials [17]. The electrical conductivity is improved by increasing the charge carrier. This will be done by doping the TE materials with the dopant that has one or more valence electrons than the host atom [1, 18]. The electrical conductivity is given by the equation:

$$\sigma = ne\mu \quad (4)$$

Where  $n$  is the charge carrier density or concentration,  $\mu$  is the mobility of charge carriers, and  $e$  is the charge of the unit carrier (electron or hole). However, doping the host atom can reduce electron mobility as a result of scattering.

The contribution of electronic thermal conductivity and lattice thermal conductivity affects the TE materials on both sides (positively and negatively). But lattice thermal conductivity contributes maximum values in TE materials at high temperatures. Doping the material with another constituent and minimizing the mean free path reduces the overall thermal conductivity of the TE materials which incases increases the figure of merit.

### 1.1.2. $Mg_2Si$ based thermoelectric materials and their properties

Because of abundance, low cost, low density, environmental compatibility, and thermal stability magnesium silicide and based alloys are preferable for thermoelectric materials [19, 20]. The crystal structure of  $Mg_2Si$  is an anti-fluorite cubic structure [21] as shown in figure 1.3. This structure belongs to the space group of high symmetry with Fm-3m (225) and the experimental bandgap of this material is around 0.77 eV [22] and the bandgap from the different computational calculations is in the range of (0.2 – 0.3)eV. As mentioned in many references, magnesium silicide has an intrinsic carrier concentration from  $3 \times 10^{17} \text{ cm}^{-3}$  to  $10^{21}$  at 300 (K) and consisting of light atoms with a high symmetry structure that are strong covalently bonded, it has low electrical conductivity ( $2 \Omega^{-1} \text{ cm}^{-1}$  at 300 K) and high thermal conductivity ( $\sim 10 \text{ W m}^{-1}\text{K}^{-1}$  at 300 K). This leads to the figure of merit of pure  $Mg_2Si$  is 0.0018 at 300 K which is a very low value. Since the efficiency of this material is not significantly improved even at high temperatures the appropriate

optimization of properties is very important. In this work, the properties of  $\text{Mg}_2\text{Si}$  had been studied and its properties were improved via doping through the art of computational methodology. By doping the base materials with strontium(Sr) through substitutional at the magnesium site, the carrier concentration had reached up to  $\sim 10^{21} \text{cm}^{-3}$  at 300 K [19] which enhances the electrical conductivity. The thermal conductivity was reduced by forming scattering in the materials that had been more investigated in this work. The applications of  $\text{Mg}_2\text{Si}$  based are applicable in the areas of thermoelectric generators for the automotive industry.

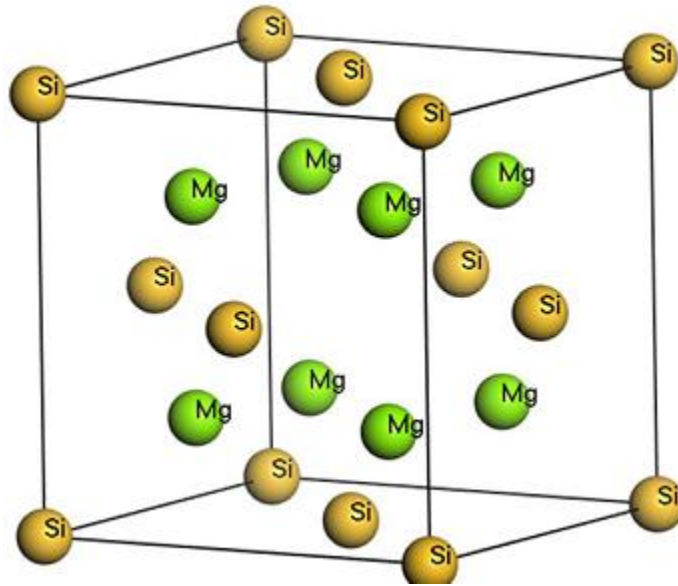


Figure 1.2 Crystal structure of  $\text{Mg}_2\text{Si}$  (ant-fluorite structure) [23]

## 1.2. Theoretical simulation

### 1.2.1. Density functional theory

From the beginning of quantum theory, the theoretical approaches for studying the properties and the application of materials have been considerably developed. This approach is mainly focused on the Schrödinger equation and studies the electronic properties of solid materials[24]. In experimental fields, the structure-property relationships have been predicted by vibrational and solid-state NMR spectroscopy through analyzing and interpreting its spectra. Such kinds of progress are focused on the electronic structure of bulk and defect sites in semiconductor materials which severe many challenges [25]. For these purposes, Density functional theory (DFT) has been



used increasingly as an exploratory tool for materials discovery and computational experiments, crystal structure prediction. Hohenberg and Kohn (1964), later generalized by Levy (1979), are the theorem that facilitates the beginning Density functional theory. According to these theorem, the all ground-state properties are functionals of the charge density [24, 26]. The density functional theory (DFT) has been proven to be an enormously powerful tool to theoretically interpret the electronic and chemical properties of materials. The principle is based on the properties of a studied system as a function of the corresponding electron density, which is promising in achieving the goal of maximizing both efficiency and accuracy of the desired electronic properties. After significant development for the past decades, DFT now has become the most widely used theory for electronic structure study [27].

In the last decades, the number of publication that contains density functional theory has significantly increased and this reveals the significance DFT to the scientific community. The success of DFT is directly related to the great compatibility of the local density approximation to the model of a homogeneous electron gas in the condensed phase.

## **1.2.2. Approximating the exchange-correlation energy**

### **1.2.2.1. Local density approximation (LDA) and General gradient approximation(GGA)**

As mentioned above, the Kohn–Sham density functional theory (KS-DFT) has been one of the most powerful quantum mechanical methods for studying the ground-state properties of atoms, molecules, and bulk materials over the past decades [28]. However, due to the exact exchange–correlation (XC) energy, functional  $E_{xc}$  in KS-DFT is unknown, many trials have been done to improving the accuracy of approximate XC energy functionals. The local density approximation (LDA) for the XC energy functional,  $E_{xc}$  LDA, has been developed from an important system called a uniform electron gas (UEG). However, a problem associated with the LDA is the self-interaction error (SIE) [29] which can be efficiently reduced by incorporating the Hartree–Fock (HF) exchange energy  $E_{x}$  HF into the LDAXC energy functional  $E_{xc}$  LDA.

The electron density can be satisfactorily described with the LDA functional when dispersion or correlation effects are not strong which is common in solid-state materials [30]. More sophisticated approximations based on LDA, such as generalized gradient approximation (GGA) or hybrid functionals, have been proposed during the past decades and have shown significant improvement

in predicting the electronic structure of molecules [28, 29]. It is also shown that hybrid functionals also have a better description of the bandgap of condensed phase semiconductors. One of the enormously popular programs of DFT, which implementing many functions is the Quantum-ESPRESSO software package. So this quantum espresso software was highly implemented in this work.

### 1.2.3. Electronic structure calculation

The structure of atoms, crystals, molecules, surfaces, and their interactions are calculated by Density Functional Theory (DFT) [31]. It is based on Hohenberg and Kohn and Sham approximation which may follow the local density approximation (LDA) or the generalized gradient approximation (GGA) to produce accurate results, for many structural and energetic properties of bulk materials and surfaces, interfaces, and point defects. Physical properties of molecules take their origin in electron assembly phenomena. To understand these properties, one has to investigate electron distributions and interactions which is contained in the electronic wave function governed by Schrödinger's equation:

$$\hat{H}\Psi = E\Psi, \quad (5)$$

Which is defining the N-electron Eigen function  $\Psi$  and eigenvalue  $E$  of the Hamiltonian  $\hat{H}$ . Hamiltonian  $\hat{H}$  is given by,  $H = \frac{p^2}{2m} + V(r)$  for a single electron. Not all values for the energy are allowed and one calls the allowed values eigenvalues. The functions  $\Psi$  which belong to the eigenvalues and which are a solution of the vibration equation and, in addition, satisfy the boundary conditions, are called Eigen functions of the differential equation. The non-relativistic Hamiltonian is written as a sum of different kinetic and potential contributing arising from interacting electrons and nuclei:

$$\hat{H} = T_N + T_e + V_{Ne} + V_{ee} + V_{NN} \quad (6)$$

Where  $T_N$ ,  $T_e$ ,  $V_{Ne}$ ,  $V_{ee}$ , and  $V_{NN}$  are kinetic energy of nuclei, the kinetic energy of an electron, interaction potential between nuclei and electrons, interaction potential between electrons and electrons, and interaction potential between nuclei and nuclei.

According to the Born-Oppenheimer approximation (BOA) the nuclei are considered motionless due to their masses are much heavier than the electrons and their kinetic energy is much smaller and the problem is solved by considering only the electronic part of the Hamiltonian. Thus, the electronic Hamiltonian using atomic units given as:

$$\hat{H}_{elec} = \sum_i \left( -\frac{1}{2} \Delta_i \right) - \sum_i \sum_A \frac{Z_A}{r_{iA}} + \frac{1}{2} \sum_{j \neq i} \sum_j \frac{1}{r_{ij}} \quad (7)$$

While the first two terms are mono-electronic, the third one is the electron-electron repulsion which excludes any analytical resolution of the many-body problem. Generally, DFT calculations allow investigating the electronic structure of nanomaterials and thus predicting their intrinsic properties, assist their characterization, rationalize the experimental results, and predict the potential application. The main equation of DFT was explained by Kohn-Sham. In this case, two theorems postulate the properties of any system. The first theorem explains as the ground state energy is the unique function of electron density i.e.  $E_0 = E(n_0(r))$  while the second theorem describes the electron density that minimizes the energy of the system as true ground electron density. based on this theorem if someone gets the electron density of the system it is easy to calculate the ground energy and know all properties of the system at ground states. The overall Kohn-sham equation is given as:

$$\left[ -\frac{1}{2} \nabla^2 + V_{ext}(r) + V_H(r) + V_{xc}(r) \right] \varphi_i(r) = E \varphi_i(r) \quad (8)$$

Where  $V_{xc}$  is exchanging correlation potentials that make difference from the previous formula.

#### 1.2.4. Energy formation

Energy formation is the potential energy due to the creation of vacancy or point defect in the system provided by the DFT code. It is the potential energy within the framework of the Born-Oppenheimer approximation. It can be calculated from the total energy of the system and the total energy of its constituent parts by fixing the nuclei and calculate the energy of the system as the sum of the kinetic energy of the electronic cloud and the energies from the Coulomb interactions between electrons and nuclei. The formed energy between the base materials and dopant atoms are calculated as:

$$\Delta E_{\text{Mg site}} = E(\text{Mg}_{2-3x}\text{SiA}_{3x}) + 3xE(\text{Mg}_2) - E(\text{Mg}_2\text{Si}) - 3xE(\text{A}) - E(\text{Mg}_2\text{Si}) \quad (9)$$

$$\Delta E_{\text{Si site}} = E(\text{Mg}_2\text{SiA}_{1-3x}\text{A}_{3x}) + 3xE(\text{Si}) - E(\text{Mg}_2\text{Si}) - 3xE(\text{A}) \quad (10)$$

$$\Delta E_{4b \text{ site}} = E(\text{Mg}_2\text{SiA}_{3x}) - E(\text{Mg}_2\text{Si}) - 3xE(\text{A}) \quad (11)$$

The above Equations correspond to the Mg, Si, and 4b sites occupied by atoms A= (Sr), and E represents the total energy values calculated.

### 1.2.5. K-Points

K-point grid is a sampling point in the Brillouin zone that arises from the Bloch theorem. For our calculation, the K-points file has used to specify the Bloch vectors (k-points) to sample the Brillouin zone. Different mechanisms can specify the k-point grids in the K-points file. These can be by automatically generating a regular mesh of points, utilizing the beginning and end-points of line segments, or as an explicit list of points and weights. The actual values of the have optimized by quantum espresso code in SCF calculation and CASTEP code in Materials studio software and the optimized value had reported for other calculation purposes [55]. In the bulk solids, the boundary conditions are used to determine the set of k-points in which the electronic states are allowed. An infinite number of k-points are accounted for an infinite number of electrons in the periodic solid. The problem of calculating an infinite number of electronic wave functions at an infinite number of k-points is solved by Bloch theorem changes. Block changes calculating a finite number of wave functions at an infinite number of k-point. Since occupied states at each k-point contribute to the electronic potential, an infinite number of calculations are needed. However, the electronic wave functions that are very close together at k-points will be almost identical. This suggests that the DFT expressions that contain a sum over k-points can be efficiently evaluated using a numerical scheme that performs summation over a small number of special points in the Brillouin zone. In addition, symmetry considerations suggest that only k-points within the irreducible segment of the Brillouin zone should be taken into account. Several prescriptions exist for generating such points and corresponding weights to be used in the summation. Using these methods, one can obtain an accurate approximation of the electronic potential and the total energy of an insulator by calculating electronic states at a very small number of k-points [56]. The calculations for metallic systems require a more dense set of k-points to determine the Fermi level accurately.

The magnitude of any error in the total energy due to limited k-point sampling can always be reduced by using a denser set of k-points, in much the same way as the convergence concerning the number of basis set functions is achieved. It is important to achieve high convergence concerning the k-point sampling when the energies of two systems with different symmetries are compared, for example, if you are looking at the relative stabilities of an FCC and an HCP structure [57]. There is no cancellation of errors in this case and both energies have to be converged. One of the most popular schemes for generating k-points was proposed by Monkhorst and Pack (1976). This scheme, which was later modified to include hexagonal systems [55], produces a uniform grid of k-points along the three axes in reciprocal space. The total energy is not variational concerning the number of k-points, so it can go up as well down in the convergence tests. This is different from the convergence concerning the cutoff energy of the plane-wave basis set, where the total energy should always decrease when the size of the basis set is increased.

### 1.2.6. Electronic transport properties

The raises of the power factor and maintains the high performance of the TE materials introduced by Seebeck effect  $S$  because the Seebeck coefficient highly depends on carrier concentration [32]. The energy difference between the average energy of the mobile carrier and the Fermi energy is  $S$  as defined in the kinetic definition of  $S$  [33]. That is as the carrier concentration  $n$  increases the Fermi energy and the average energy increase. But the increment of Fermi energy is higher than that of average energy. Consequently, the Seebeck effect decreases, and the power factor ( $S^2 \sigma$ ) decreases rapidly. Thus to increase the  $ZT$  of thermoelectric Materials, the carrier concentration ( $n$ ) increases electrical conductivity( $\sigma$ ) but reduces the Seebeck coefficient( $S$ ) [34]. According to the Boltzmann transport equation, the Seebeck effect is related to carrier concentration as follow;

$$S = \frac{8\pi^2 k_B^2}{3eh^2} m^* T (\pi/3n)^{\frac{2}{3}} \quad (12)$$

Where ' $k_B$ ' is Boltzmann constant, ' $h$ ' is plank constant, ' $m^*$ ' is effective mass and ' $e$ ' is carrier electron. From this equation, the Seebeck effect is related to carrier concentrating by;  $S \approx \left(\frac{\pi}{3n}\right)^{\frac{2}{3}}$  which is an inverse relationship. In addition to Seebeck, the relation between electronic thermal conductivity  $\kappa$  and  $n$  is also another complicated term. Electronic thermal conductivity is related to electrical conductivity  $\sigma$  by the Wiedemann–Franz law. It is given by;

$$\kappa_e = L\sigma T \quad (13)$$

Where  $L = 2.44 \times 10^{-8} \text{ W}\Omega \text{ K}^{-2}$  is Wiedemann–Franz constant

### 1.2.6.1. Electronic Bandstructure

In a solid, the band structure describes the range of energy levels that electrons may have within it, as well as the ranges of energy that they may not have (called band gaps or forbidden bands). The combination of bands and band gaps describes the band structure in band theory by examining the allowed quantum mechanical wave functions for an electron in a large, periodic lattice of atoms or molecules. The physical properties such as optical absorption, electrical resistivity, and electrical conductivities are successfully described by Band theory.

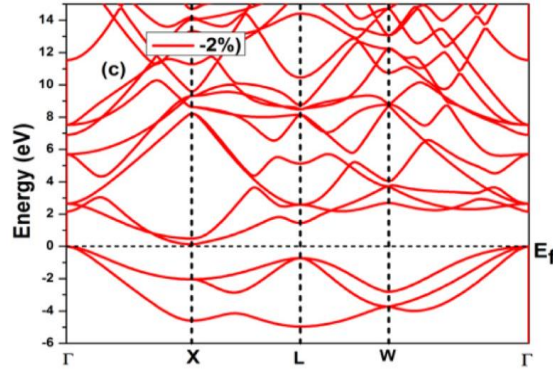


Figure 1.3 Electronic band structure of Mg<sub>2</sub>Si under compressive strain [35]

### 1.2.6.2. The density of states (DOS) and partial density of states (PDOS)

#### 1.2.6.2.1. The density of states (DOS)

The density of states (DOS) for a given band  $n$ ,  $N_n(E)$ , is defined as:

$$N_n(E) = \int \frac{dk}{4\pi^3} \delta(E - E_n(k)) \quad (14)$$

Where  $E_n(k)$  describes the dispersion of the given band and the integral is determined over the Brillouin zone. An alternative representation of the density of states is based on the fact that  $N_n(E) dE$  is proportional to the number of allowed wave vectors in the  $n$ th band in the energy range  $E$  to  $(E + dE)$ . The total density of states,  $N(E)$ , is obtained by summation over all bands. The integral of  $N(E)$  from minus infinity to the Fermi level gives the total number of electrons in the unit cell

[36, 37]. In a spin-polarized system, separate DOS for electrons with spin up and spin down can be introduced. Their sum produces the total DOS and their difference is referred to as the spin density of states. The DOS is a useful mathematical concept, allowing integration concerning electron energy to be used instead of integration over the Brillouin zone. In addition, the DOS is often used for quick visual analysis of the electronic structure. Characteristics such as the width of the valence band, the energy gap in insulators, and the number and intensity of the main features are helpful in qualitatively interpreting experimental spectroscopic data. DOS analysis can also help to understand the changes in electronic structure caused by, for example, external pressure.

There are a variety of numerical techniques for evaluating the DOS. The simplest one is based on the Gaussian smearing of the energy levels of each band, followed by a histogram sampling. This method does not reproduce sharp features of the DOS, such as van Hove singularities, but it does satisfactorily reproduce the general shape of the DOS, even when only a small number of k-points are used. The most popular and reliable technique is unfortunately not well suited to the Monkhorst-Pack grid of special points, which is based on tetrahedron interpolation. So, CASTEP uses a simplified linear interpolation scheme which is based on linear interpolation in parallelepipeds formed by the points of the Monkhorst-Pack set.

#### **1.2.6.2.2. Partial and local density of states (PDOS)**

Partial density of states (PDOS) and local density of states (LDOS) represent useful semi-qualitative tools for analyzing electronic structure shows the atoms that contribute various parts of the energy spectrum to electronic states in the system were qualified by LDOS. While these results are qualified by PDOS by resolving the contributions according to the angular momentum of the states. It is often useful to know whether the main peaks in the DOS are of s, p, or d character [38]. The Mulliken population analysis allows the contribution from each energy band to a given atomic orbital to be calculated, which is applied for PDO calculation. The summation of these contributions overall bands produces a weighted DOS

#### **1.2.7. Phonon calculations**

Thermal conductivity in crystal rises from two mechanisms of heat transportation namely lattice thermal conductivities  $k_l$  and electronic thermal conductivity  $k_e$  [33]. Electronic thermal conductivity  $k_e$  is due to electron flow in crystal and related to electrical conductivity by the

Wiedemann–Franz law:  $\kappa_e / \sigma = LT$  where  $L$  is the Lorenz number. Since the electronic thermal conductivity is very low most of the time, the lattice thermal conductivity has a greater role in the total thermal conductivity. Consequently, we are mainly focused on the reduction of lattice thermal conductivity in this research. In the solid crystal, the lattice thermal conductivity rises from phonon vibration [39]. The Boltzmann theory was adapted by Peierls to describe the transport of gases to phonon “gas” and postulating the Peierls–Boltzmann transport (PBTE) equation for calculating phonon lifetimes and  $\kappa$ , through a complex set of coupled integrodifferential equations, which is a complicated task [3]. In most cases,  $k_1$  is related to sound wave velocity and mean free path [40] and thus a doped heavy atom interfere with this variable and reduces the lattice thermal conductivity which will be studied in this research. The phonon-glass electron crystal or PGEC is to disrupts the phonon transport properties without affecting electron transport. The disruption of phonon thermal conductivity is occurred by a well-known technique called, alloying and nano-structuring [32]. This shows materials with a low thermal conductivity as in glass and high electrical conductivity as in crystal were preferred as the best thermoelectric materials [6]. So reducing the lattice thermal conductivity and optimizing the carrier concentration  $n$ , by introducing a scattering center were the normal way of optimizing the TE materials. Generally to calculate lattice thermal conductivity many packages like ShengBTE, phon03py, phonopy, etc are available. Among them, phono3py is the best code for accurately calculate the lattice thermal conductivity based on the direct solution of the linearized Boltzmann transport equation (LBTE) or based on relaxation time approximation (RTA). We have used RTA in this thesis to calculate lattice thermal conductivity. Calculating through RTA has a complicated equation that is guided in phono3py. It also gives the physical properties like phonon lifetime/line width, the imaginary part of self-energy, and joint density of states. However, we have only considered the relationship between phonon lifetime imaginary part of the energy and lattice thermal conductivities.

#### **1.2.7.1. Phonon lifetime calculation**

The Relaxation Time Approximation (RTA) solves the problems non-diagonal form of the collision. The solution is performed by assuming the rate at which a phonon wave vector ( $\mathbf{q}$ ) relaxes does not depend on the non-equilibrium situation of the phonons colliding with it. Phonon lifetime is calculated from imaginary self-energy and its full expression is written in Appendix A.



Assume if the imaginary part of self-energy is represented by,  $\Gamma_\lambda(\omega_\lambda)$  the inverse of it gives the relaxation time;

$$\tau_\lambda = \frac{1}{\Gamma_\lambda(\omega_\lambda)} \quad (15)$$

### 1.2.7.2. Lattice thermal conductivity calculation

In the Boltzmann transport equation, the lattice thermal conductivity  $\kappa$  is calculated based on relaxation time (RTA) as follows;

$$\kappa = \frac{1}{NV_0} \sum_\lambda C_\lambda v_\lambda \otimes v_\lambda \tau_\lambda \quad (16)$$

where  $N$  is the number of unit cells in the system,  $V_0$  of the volume of the unit cell, the symbol  $\lambda$  represents the phonon mode as the pair of phonon wave vector  $q$ ,  $v_\lambda$  is group velocity and  $C_\lambda$  is the mode heat capacity which given as;

$$C_\lambda = K_B \left( \frac{\hbar\omega_\lambda}{K_B T} \right)^2 \frac{\exp\left(\frac{\hbar\omega_\lambda}{K_B T}\right)}{\left[\exp\left(\frac{\hbar\omega_\lambda}{K_B T}\right) - 1\right]^2} \quad (17)$$

Where  $\omega_\lambda = \omega(q,j)$  is the phonon frequency,  $T$  is the temperature, and  $\hbar$  denote the reduced Planck constant. The group velocity is calculated as;

$$v_\alpha(\lambda) \equiv \frac{\delta \omega_\lambda}{\delta q_\lambda} \quad (18)$$

### 1.3. Statements of problem

Even though most thermoelectric materials like  $\text{Bi}_2\text{Te}_3$ ,  $\text{PbSn}$ , etc have a high figure of merit  $ZT$ , the abundance and toxicity of these materials are great problems for effective use. To overcome this problem the development of thermoelectric materials based on  $\text{Mg}_2\text{Si}$  is highly investigated in recent research areas. But due to the low  $ZT$  values of these materials, their applications were limited to lower areas such as refrigerators, a cooling device for laser diodes, and cooling seats in automobile cooling systems. From the invention of  $\text{Mg}_2\text{Si}$  to the recent year the  $ZT$  value of these TE materials did not develop to high values [20, 41]. The low value of  $ZT$  is due to the interdependence of intrinsic properties of its parameters like electrical conductivity, Seebeck coefficient, thermal conductivity, and electronic thermal conductivity [42]. As mentioned in many references the improvement of electrical conductivity by increasing carrier concentration minimizes the Seebeck coefficient and increases electronic thermal conductivity, which negatively affects the figure of merit and prohibits its improvement for more than a century. However, minimization of lattice thermal conductivity is the best criteria to maximize a  $ZT$  value which had studied in this research by a theory-guided approach and computational methods (first principle calculation based on density functional theory (DFT)).

### 1.4. Scopes

The main focus of this thesis is the investigation of the effects of heavy doping on the efficiency of thermoelectric based on  $\text{Mg}_2\text{Si}$ . The efficiency of thermoelectric materials is studied interims of the figure of merit  $ZT$ . The lattice thermal conductivity is calculated by varying the constituents of the dopant atom and lastly, the good figure of merit had reported by the characterization of electronic structure and properties using first principle calculation based on density functional theory (DFT) and Semi-classical Boltzmann theory. However, the calculation of relaxation time was very complicated, estimation based on references will have taken to estimate the exact values of thermoelectric power or the figure of merit. This work is limited to study the theoretical properties and enhancement of the efficiency of doped  $\text{Mg}_2\text{Si}$  by simulating at the level of atomistic and electronic scale, which doesn't involve any experimental work. The computational costs were also limit us to use fewer supercell (2x1x1) and low k-point grids.

## 1.5. Objective

The main objective of this research was to minimize the lattice thermal conductivity for good TE performance by substitutional doping of strontium (Sr,) in the Mg site to the Mg<sub>2</sub>Si-based thermoelectric material.

### 1.1.2. Specific objectives

The specific objective of this research is:

- To optimize the parameters (lattice constant, Energy cutoff, charge density cutoff, and k-point grid)
- To calculate the band structure, density of state, and carrier density for each doped and undoped Mg<sub>2</sub>Si
- To calculate the lattice thermal conductivities, electrical conductivities, Seebeck coefficient, and electronic thermal conductivity for each doped Mg<sub>2</sub>Si

## 2. LITERATURE REVIEWS

### 2.1 Introduction

The overall properties of thermoelectric materials are governed by basic parameters such as thermal conductivity, electrical conductivity, Seebeck coefficient, and temperature [40]. The combination of these parameters gives the figure of merit, which determines the efficiency of thermoelectric materials. Thermoelectric materials with a high figure of merit have high efficiency. But the interdependence of intrinsic properties of thermoelectric materials thermal conductivity ( $k_e$ ) which influences the ZT of thermoelectric materials prohibits the development of these materials and leads to low efficiency. As mentioned in the reference [3, 25] the Seebeck coefficient of thermoelectric materials is related to effective mass and carrier concentration. By another way, the figure of merit (ZT) of thermoelectric (TE) materials has a square proportional to the Seebeck coefficient and linearly proportional to the electrical conductivity. But it has an inverse relationship to thermal conductivity. According to this relationship enhancing the ZT of thermoelectric materials needs the reduction of thermal conductivity and the increment of Seebeck coefficient and electrical conductivity. The overall thermal conductivity in solid crystals is resulted from thermal conductivity ( $k$ ) due to electron ( $k_e$ ) and thermal conductivity due to lattice vibration ( $k_l$ )[18]. The thermal conductivity due to electrons is related to electrical conductivity by the well know Wiedemann–Franz Law [1]. From this, we understand that increasing the electrical conductivity can increase the electronic thermal conductivity which negatively affects the ZT value. On the other hand, the electrical conductivity is enhanced by increasing the charge carrier by doping with other appropriate elements. However, the increment of charge carrier leads to the reduction of the Seebeck coefficient which reduces highly the ZT of TE materials [42]. From this observation, we can consider the improvement of the ZT of TE materials is very difficult due to the interdependence of the intrinsic properties of these materials. To improve these properties many researchers are focused on different mechanisms to acquire the best thermoelectric efficiency. Among these, TE materials based on  $Mg_2Si$  [22] ] are the recent research area due to the low cost of production, non-toxicity, and good thermal stability.

## 2.2 Theoretical Review for Enhancing Thermoelectric Materials

### 2.2.1 Enhancing ZT in bulk materials

The best thermoelectric materials are the materials that should have a low lattice thermal conductivity as in a glass, and a high electrical conductivity as in a crystal. Since the interdependence of thermoelectric materials is challenging, the normal techniques of managing are to enhance the power factor by optimizing the carrier concentration or to reduce the lattice thermal conductivity  $k$  by creating the scattering centers [6, 8]. In bulk materials, alloying and/or doping is the major approach to improve the thermoelectric properties by altering the lattice thermal conductivity without affecting the electrical conductivity [43]. Typically heavily doped semiconductors with low thermal conductivity can behave as a good thermoelectric material with high ZT [44, 45]. For Example, the figure of merit of  $\text{Mg}_2\text{Si}$  reaches  $ZT = 2.96$  for p-type at 800 K and 1.68 for n-type at 1000 K by optimum doping of Ba,[41] which reduces the thermal conductivity by a large factor. In addition, the effect of heavy elements on ZT values is also reported in ref[42]. It also explains as the mass fluctuation in lattice crystal due to heavy elements enhances the ZT values by creating point defects, which minimizing the phonon-free path. According to reference[22], the pure  $\text{Mg}_2\text{Si}$  has a ZT of less than 0.002 which later enhanced by doping with elements such as Sn, Ge, Sb, and Bi, and reported a maximum ZT value of 1.2 T = 700 K for  $\text{Mg}_2\text{Si}_{0.6}\text{Sn}_{0.4}$  and  $ZT_{\text{max}} = 0.7 - 0.86$ , T = 823–862 for  $\text{Mg}_2\text{Si: Bi}_{0.02}$  [13]. This property again enhanced  $ZT_{\text{max}}$  by n-type doping up to 1.4, at T = 823 K for  $\text{Mg}_2\text{Si}_{0.53}\text{Sn}_{0.4}\text{Ge}_{0.05}\text{Bi}_{0.02}$  and 0.5 by p-type doping at the temperatures of 300K [13, 18]. Besides the experimental technique, the computational methods are highly applicable in recent progress to study the electronic properties and mechanism needed to improve this complexity [25, 27]. From all these references we conclude that minimizing the lattice thermal conductivity, which enhances the performance by high value [39, 41] is preferable relative to an increment of carrier concentration

### 2.2.2 Novel approach

The novel approach is a strategic method used to minimize the lattice thermal conductivity without affecting electrical conductivity. The most widely adopted methods to minimize lattice thermal conductivity are phonon scattering, using complex structures to separate electron crystal from phonon glass, mixing multiphase on low dimensional materials [3, 46]. In the phonon scattering

approach, scattering can be achieved in different frequency ranges by a mechanism such, mass fluctuation scattering, grain boundary scattering, and interface scattering with thin films [42]. The Complex crystal structures are also used to minimize lattice thermal conductivity by separating Electron- crystal from phonon-Glass which is sometimes called the phonon-glass electron-crystal (PGEC) approach [6]. Such kind of materials has the structures contain large voids. These voids can be filled with loosely bound atoms which leads to reduces phonon lifetimes. They also have the valence-balanced combination of cations and covalently bonded anionic units. This combination leads to higher charge mobilities than purely ionic compounds and large, complex unit cells with intrinsically low thermal conductivity [42].

### **2.2.3 Mass fluctuation technique (Half Heusler Materials)**

Half Heusler compounds which contain many semiconductor materials are the best group of materials for the application of high temperature thermoelectric. In recent progress, these materials achieve good performance and have high ZT values above 1000 K in TE materials. It appears as both n-type  $\text{MNiSb}$  ( $\text{M} = \text{Ti, Zr, Hf}$ ) and p-type  $\text{FeRSb}$  ( $\text{R} = \text{V, Nb}$ ) HH compounds [47]. It has been reported that the high content of heavier Hf dopant minimizes thermal conductivity without affecting the other thermoelectric properties. The reduction of lattice thermal conductivity enhanced by both the electron-phonon scatterings and point-defect [48], which is very important for thermoelectric application, was reported in these materials. Half Heusler Materials have shown good material stability, high power density, and has also a high power factor. However, the dimensionless figure of merit (ZT) of these materials is near 1 for a long time due to their high thermal conductivity [49]. Consequently, the ZT value of these materials has improved to 1.5 since 2013, in the temperature range of 500–900 K for both n- and p-type compounds [50, 51].

### **2.2.4 Nanostructured thermoelectric**

Another approach to improve low-cost bulk materials with poor thermoelectric properties which have been considered for many years was reduced dimensionality[6]. Enhancement of the DOS near the Fermi level throughout the quantum confinement and increasing the presence of interfaces and surfaces are the two distinct mechanisms being developed for improving the thermoelectric properties of a material using nanostructured morphologies [42, 52]. Quantum confinement

enhances the thermo-power by increasing the electronic DOS near the Fermi level while the presence of phonon scattering at the surface and interface enhances scatter of heat-conducting phonons without reducing electronic conduction [53]. Through the possible enhancement of the power factor, Nanostructured semiconductors have been widely investigated as the method for increasing  $ZT$  or the reduction of the thermal conductivity of the lattice [33]. From a practical perspective, increasing the  $ZT$  throughout modulation doping and quantum confinement is the best method while it has been found recently that dimensional restriction can lead to a much-enhanced efficiency over traditionally used bulk thermoelectrics [54]. So that dimensional restriction is also the best method to improve the efficiency of thermoelectric properties.

### 3. COMPUTATIONAL METHODS

The overall works and all calculations for this thesis were performed in different categories. These were; Geometry optimization, Bandstructure and DOS of calculation, Elastic properties calculation Electronic properties calculations, and phonon properties calculation. Geometry optimization contains the optimization of lattice parameters (a, b, c, and related angles), cutoff energy (plane-wave basis set), and k-point (Brillouin zone sampling). For these parameters optimization the CASTEP program which is one of the tasks in Materials Studio 2017, was used to provide an efficient implementation of DFT. In this work, our materials, are written in different forms.  $\text{Mg}_2\text{Si}$  is the reduced general forms of magnesium silicide, which has an FCC crystal structure of space group 225, Fm-3m (225),  $\alpha = \beta = \gamma = 90^\circ$  and  $a = b = c$  [23, 41, 55, 56]. It has 12 atoms per-unit cell in which 8 Mg occupies tetrahedral site 8c (0.25 0.25 0.25) and Si occupies all 4a (0 0 0) sites. We have used  $2 \times 1 \times 1$  to generate supercells. The supercell of  $\text{Mg}_2\text{Si}$  generated is written as  $\text{Mg}_{16}\text{Si}_8$ . In this work, we have used 8.33% and 16.67% of Sr substitutional doping along Mg-site, which has 1Sr and 2Sr in unit cell respectively. The expression of supercell for 8.33% is  $\text{Mg}_{14}\text{Si}_8\text{Sr}_2$  and  $\text{Mg}_{12}\text{Si}_8\text{Sr}_4$  for 16.67%. So we have used to express  $\text{Mg}_8\text{Si}_4$ ,  $\text{Mg}_7\text{Si}_8\text{Sr}$  and  $\text{Mg}_6\text{Si}_8\text{Sr}_2$ , in a unit cells for undoped, 8.33% and 16.67% Sr doped respectively. Only one lattice parameter (celldim)(1) was optimized and the possible k-point grids were adjusted for superstructures to simulate approximation. The calculations for lattice dimensions were performed by fixing both the cutoff and k-point grid. As explained in CASTEP dialogs, the cutoff has to be settled to maximum energy. To optimize the lattice dimension, the k-point was fixed to  $4 \times 4 \times 4$  and the cutoff energy was fixed to 380 eV. After minimum energies were acquired the optimum value of lattice dimension was taken and another task for cutoff and k-point calculations were provided with the same steps. In all calculations, the DFT calculations with the projector augmented-wave (PAW) method were used to describe interactions between electrons. For the exchange-correlation potential, the general-gradient approximation (GGA) in the Perdew–Burke–Ernzerhof (PBE) prescription was used. In this calculation  $2 \times 1 \times 1$  supercell was generated by CASTEP and SCF with the convergence criteria for energy tolerance of  $10^{-6}$  eV/atom was chosen between consecutive steps. The CASTEP implementation involves a Hessian in the mixed space of internal and cell degrees of freedom so that both lattice parameters and atomic coordinates can be optimized. For this Broyden-Fletcher-Goldfarb-Shanno (BFG) minimizer was used. OTFG



Ultrasoft was used to specify pseudopotentials of elements. To optimize cutoff Fast Fourier Transformation (TTF) with a density standard of  $30 \times 30 \times 30$  was used to maintain the efficient way to transform various entities between Hamiltonian and exchange-correlation function.

After geometry optimization, Bandstructure and DOS were calculated by using CASTEP again. To calculate Bandstructure and DOS,  $2 \times 2 \times 2$  and  $4 \times 4 \times 4$  k-points were used for supercell and unit cell respectively. From the optimized unit cell, the lattice dimension was chosen at  $6.3562 \text{ \AA}$ . The plane-wave cutoff energy for all calculations of the unit cell was set to 330 eV. The medium k-point separation ( $0.025/\text{A}^0$ ) and band energy tolerance of about  $10^{-5}$  eV were also used to perform all structural calculations.

The electronic Transport properties include properties such as electrical conductivity, Seebeck coefficient, and electronic thermal conductivity. For these properties, the Boltzmann transport theory was implemented. Specifically, the BoltzTrap code with Quantum Espresso was used to calculate all these properties as shown in appendix A. GGA –PBE was used for exchange-correlation potential calculation. For both native  $\text{Mg}_{16}\text{Si}_8$  and Sr-doped ( $\text{Mg}_{14}\text{Si}_8\text{Sr}_2$ ,  $\text{Mg}_{12}\text{Si}_8\text{Sr}_4$ ).  $2 \times 1 \times 1$  supercell was used for nSCF calculation that contains 24 atoms. The Brillouin zone was sampled by  $18 \times 18 \times 18$  Monkhorst–Pack k-point mesh (46 points in irreducible Brillouin zone) for electronic part calculation by using BoltzTrap code. The result of nSCF calculation was used to generate a file that contains all electronic transport properties by BoltzTrap code in python code and the output file was extracted to each parameter (Seebeck, electrical conductivity, electronic thermal conductivity). The Seebeck coefficient and electrical conductivity were calculated based on the relaxation time approximation by using Boltzmann transport equation BTE electron after calculating the carrier concentration and its distribution responding to temperature and chemical potential.

Lattice thermal conductivity (phonon calculation) was done by Phono3py code and implemented in the Boltzmann transport equation of each structure calculation. For this nSCF calculation with  $6 \times 6 \times 6$  k-point was used and  $2 \times 1 \times 1$  supercell was generated for all  $\text{Mg}_{16}\text{Si}_8$  and Sr-doped ( $\text{Mg}_{14}\text{Si}_8\text{Sr}_2$ ,  $\text{Mg}_{12}\text{Si}_8\text{Sr}_4$ ). SCF calculation of each super cell was implemented for the calculation of force constants. . Its main inputs are sets of second-and third-order interatomic force constants. The second-order force constant is used to compute frequency, phonon distribution function and

velocity, while the third-order force constant measures the relaxation time and measure of deviation based on the equations in Appendix B. For second-order IFCs, calculation of the results from SCF of Phono3py was directly used, but for third-order IFCs, a  $2\times 1\times 1$  supercell was built and the calculation was implemented. After all, constant forces were collected  $2\times 1\times 1$  dimension and  $25\times 25\times 25$  q-point mesh were used to calculate lattice thermal conductivity.

## 4. RESULT AND DISCUSSION

### 4.1 Optimization and stability of crystal structures

First-principles properties calculation is based on the information of crystals. This information is the crystal structure, plane-wave energy cutoff, k-point grids, and lattice dimensions. In this work these all parameters have been optimized before any calculations had been done. After optimization, the lattice parameters of  $\text{Mg}_8\text{Si}_4$  were fixed to  $6.3562 \text{ \AA}$  as shown in figure 4.1(c) which is very similar to the previous computational work [23, 36, 38] and experimental work ( $6.385 - 6.393 \text{ \AA}$ ) [57, 58] in unit cell. This values have increased in supercells of  $(2 \times 1 \times 1)$ . It forms ( $13.438 \text{ \AA}$ ,  $6.719 \text{ \AA}$  and  $6.632 \text{ \AA}$ ), ( $13.016 \text{ \AA}$ ,  $6.508 \text{ \AA}$  and  $6.362 \text{ \AA}$ ), ( $12.6473 \text{ \AA}$ ,  $6.3846 \text{ \AA}$ , and  $6.38467 \text{ \AA}$ ) in the lattice dimension (a,b and c) for  $\text{Mg}_{12}\text{Si}_8\text{Sr}_4$  (16.66% Sr-doped),  $\text{Mg}_{14}\text{Si}_8\text{Sr}_2$  (8.33% Sr-doped) and  $\text{Mg}_{16}\text{Si}_8$  (undoped) respectively. From this we have observed as the symmetry of the crystal was reduced by increasing the concentration of Sr-dopant. The crystal imperfection affects the electronic properties while it improves thermal conductivities, which proves our hypothesis. Similarly, k-point grid and plane-wave cutoff energy were also optimized as shown in figure 4.1(a) and (c) respectively. After parameters optimization, the stability of the  $\text{Mg}_8\text{Si}_4$  in the unit cell was checked by CASTEP code based on elastic constraints. In this paper, we have shown the stability of  $\text{Mg}_8\text{Si}_4$  by calculating elastic constant ( $C_{ij}$ ) based on Boron-Huang's lattice dynamic theory. For the cubic crystal system, the independent elastic constants  $C_{11}$ ,  $C_{12}$ , and  $C_{44}$  must satisfy the equation 15 shown below [23, 41]. As shown in Table 4.1 the stability was proved since it was satisfied the rule.

$$C_{11} > 0, C_{44} > 0, C_{11} - C_{12} > 0, C_{11} + 2C_{12} > 0 \quad (19)$$

Table 4-1 Elastic constant ( $C_{ij}$ ) of undoped and Sr-doped  $Mg_2Si$

Compounds	Elastic constant ( $C_{ij}$ )(GPa)				
	$C_{11}$	$C_{12}$	$C_{44}$	$C_{11} - C_{12}$	$C_{11} + 2C_{12}$
$Mg_8Si_4$	114.10	21.99	44.69	92.11	157.98
$Mg_7Si_4Sr$	120.11	29.17	42.91	77.20	157.98
$Mg_6Si_4Sr_2$	112.32	24.71	36.53	87.61	161.74

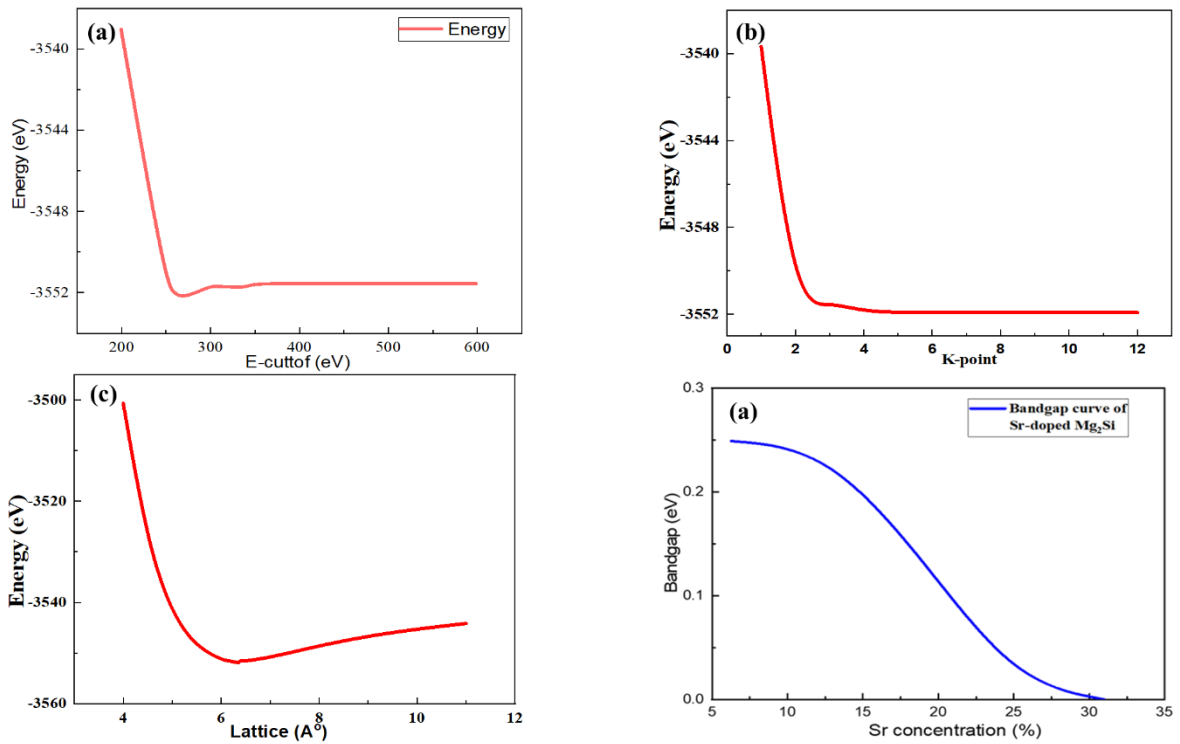


Figure 4.1 Geometry optimization a) optimized lattice) optimized k-points, c) optimized E-cutoff and, d) bandgap optimization

## 4.2 Electronic properties Analysis

### 4.2.1 Electronic Bandstructure and DOS analysis

The electronic structure and properties of  $\text{Mg}_8\text{Si}_4$ ,  $\text{Mg}_7\text{Si}_4\text{Sr}$ , and  $\text{Mg}_6\text{Si}_4\text{Sr}_2$  were computed by first-principle calculation. As shown in figure 4.2(a, b, and c) the maximum valance band coincides at Gamma (G) point while the minimum conduction band is located at X-points in the Brillouin Zone. From this, we conclude the materials are indirect bandgap. Accordingly the bandgap of  $\text{Mg}_8\text{Si}_4$ ,  $\text{Mg}_7\text{Si}_4\text{Sr}$ , and  $\text{Mg}_6\text{Si}_4\text{Sr}_2$  are 0.227 eV, 0.241eV and 0.017 eV respectively. It shows the variation of bandgap as the concentration of dopant increases as shown in figure 4.1 (d). This is due to the increment of lattice distance caused by the dopant atom. We have introduced substitutional doping in our system in which Sr was substituted by Mg, in which the atomic radius of Sr is greater than that of Mg. This creates a tensile force on neighboring atoms and leads to the increments of lattice distance. An increment of lattice distance increases the interatomic distance, which reduces the binding energy. From the definition of bandgap energy, electrons with low bound energy can be excited to conduction band with minimum energy. The minimum energy gives to electrons to be in conduction band from valance band is bandgap. The electronic structures of Mg is  $1s^2 2s^2 2p^6 3s^2$ , for Si;  $1s^2 2s^2 2p^6 3s^2 3p^2$  and  $1s^2 2s^2 2p^6 3s^2 3p^6 4s^2 3d^{10} 4p^6 5s^2$  for Sr. Introducing another new orbital to the native ( $\text{Mg}_2\text{Si}$ ) increases the bandstructure energy of electrons near Fermi energy. The density of the state of doped compounds is greater than undoped compounds as shown in figure 4.2 (d), (e), and (f). This is due to introducing a new  $5s^2$  from Sr atom to the system. Electron with higher energy occupies the higher position. Most of  $3s^2$  from Mg and Si occupy around the energy level of -5ev to 0. However, the 3p from Si and 4s from Sr occupy above Fermi level (0 eV).

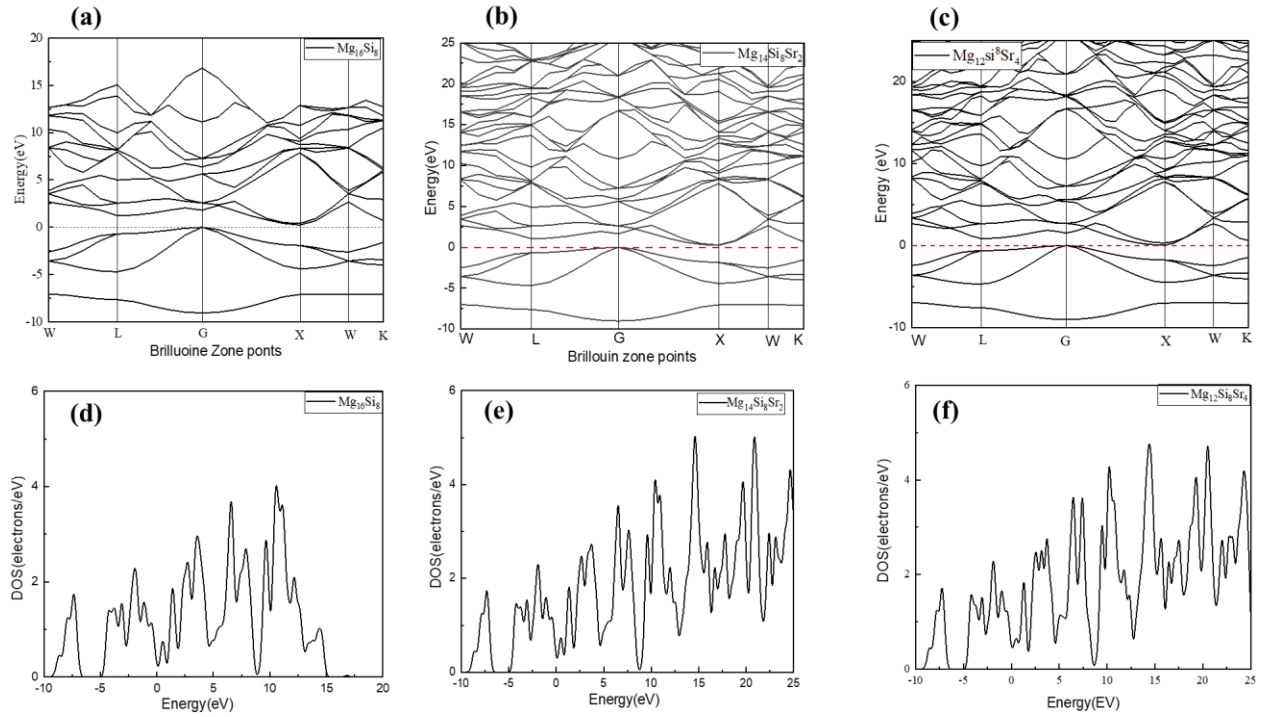


Figure 4.2 Bandstructure and DOS of  $Mg_{16}Si_8$  (a and d),  $Mg_{14}Si_8Sr_2$  (b and e), and  $Mg_{12}Si_8Sr_4$  (c and f) respectively

#### 4.2.2 Electronic transport properties

The objective of our work in this thesis is to reduce the lattice thermal conductivity by optimizing other properties like Seebeck coefficient electrical, conductivity, and electronic thermal conductivity. We have achieved our goal by introducing substitutional doping of Sr atom to  $Mg_2Si$ . We have done by calculating all these properties of the native compound and relatively compared it with the doped one by varying the concentration of the dopant atom. The electrical conductivity, Seebeck coefficient, and electronic thermal conductivity of un-doped  $Mg_2Si$  were calculated by BoltzTrap code which is implemented by the Boltzmann transport equation. All equation used for this code is described in appendix A. The results of the Seebeck coefficient, electrical conductivity, and electronic thermal conductivity were shown in figures 4.3 (a), 4.4 (a), and 4.5(a) respectively. After we had known the properties of the native compound, we had calculated the properties of

the doped compound by using BoltzTrap code again. For undoped  $\text{Mg}_{16}\text{Si}_8$ , the contribution of electron and holes are almost similar as the temperature increases but the Seebeck coefficient continuously increases with temperature for p-type for all chemical potentials as shown in figure 4.3 a).

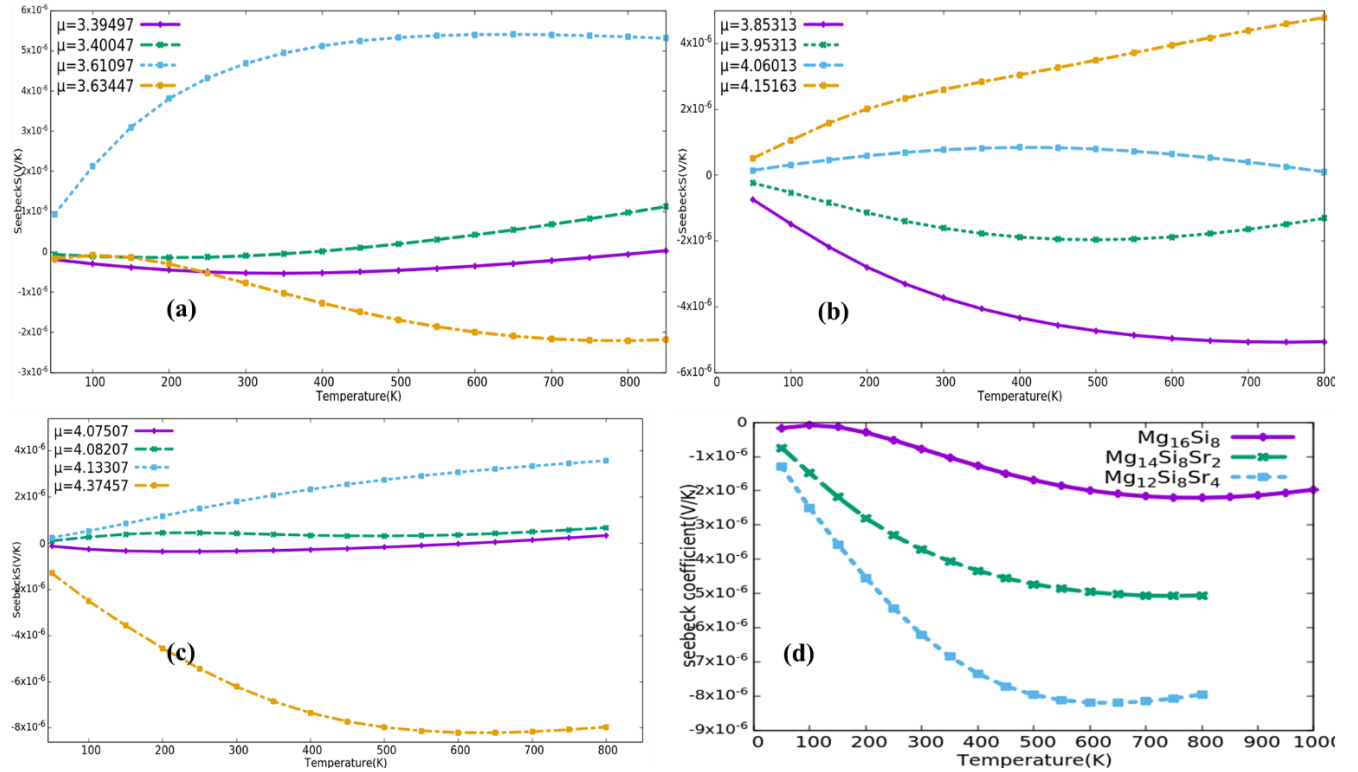


Figure 4.3 Seebeck coefficients as a function of temperature and chemical potentials for; electrical conductivity (a),  $\text{Mg}_{16}\text{Si}_8$ , (b)  $\text{Mg}_{14}\text{Si}_8\text{Sr}_2$ , (c)  $\text{Mg}_{12}\text{Si}_8\text{Sr}_4$ , and (d) comparison of the three

For the doped compound ( $\text{Mg}_{12}\text{Si}_8\text{Sr}_4$  and  $\text{Mg}_{14}\text{Si}_8\text{Sr}_2$ ) the Seebeck coefficient increase with increasing dopant concentration and temperature as shown in figure 4.3(d).

The Seebeck coefficient increases more for n-type (-ve Seebeck coefficient)  $\text{Mg}_{12}\text{Si}_8\text{Sr}_4$  with temperature and reaches maximum values at 600K. It continuously increases for p-type (+ve Seebeck coefficient) with lower values than n-types. This shows that the electron contributes more to transport properties than holes. Generally, the Seebeck coefficient increases for doped compounds when related to the undoped compound. For doped compound, the contribution of

electrons is higher than holes and shows the materials behaves as n-type and behaves p-type at higher temperature(above 800K).

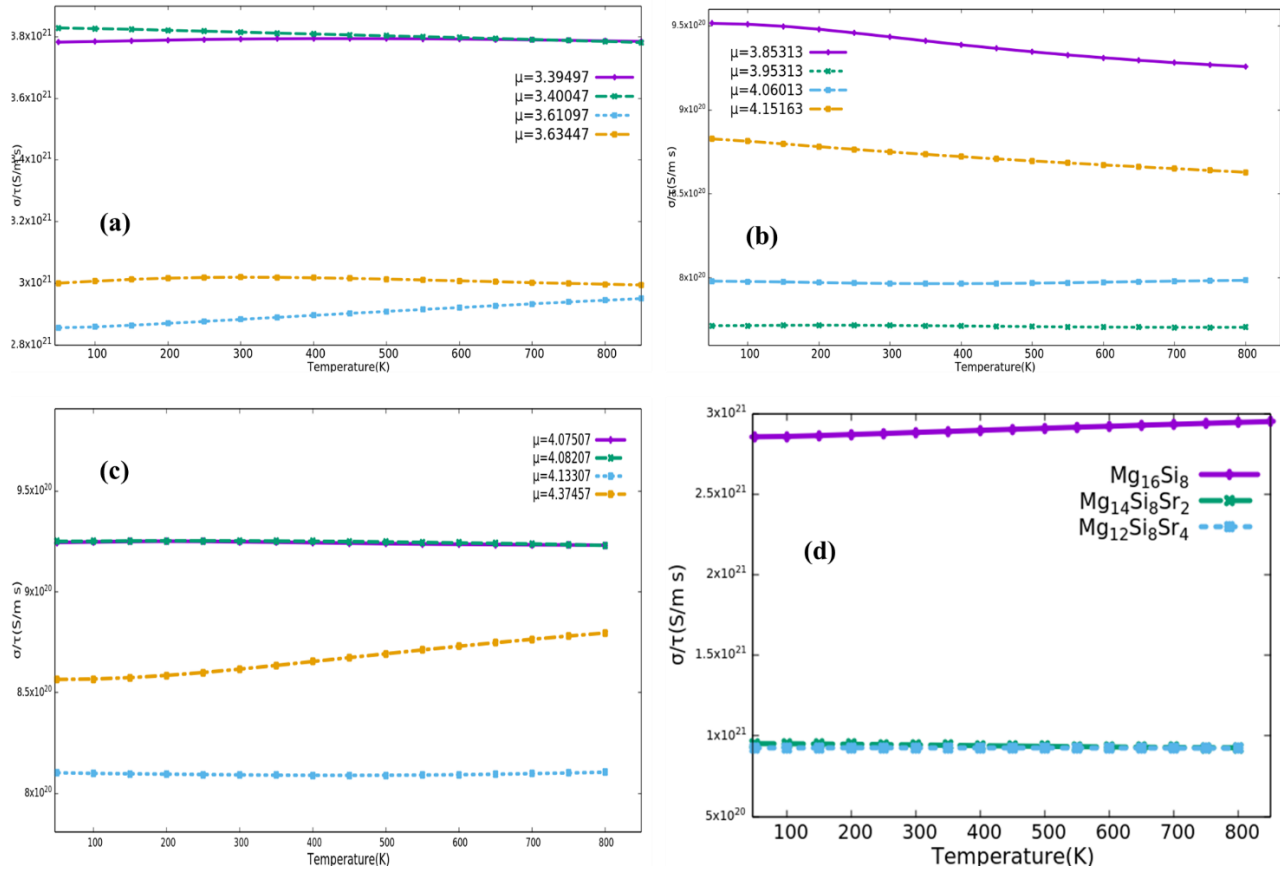


Figure 4.4 Electrical conductivity as a function of temperature and chemical potentials for; (a),  $Mg_{16}Si_8$ , (b)  $Mg_{14}Si_8Sr_2$ , (c)  $Mg_{12}Si_8Sr$ , and (d) comparison of the three

In this work, all results from the BoltzTrap code were calculated under constant relaxation time in which its exact value is not calculated. But to know the exact values of electrical conductivity and electronic thermal conductivity the effect of relaxation time is very important. To evaluate the result it is possible to estimate the relaxation time since the relaxation time  $\tau$  for most materials is in the orders of  $10^{-15}$  to  $10^{-14}$  [41]. However, this value is varied in materials due to effective mass and our estimation was roughly to check the optimization of these two properties. As shown in Figures 4.5 the electronic thermal conductivity increases with increasing temperature for all compounds. The electrical conductivities of the doped  $Mg_2Si$  were reduced due to the formation of scattering caused by the reduction of symmetry as the concentration of Sr increases. Sr doping increases the phonon scattering and reduces the carrier mobility, which reduces electrical



conductivity and electronic thermal conductivity as shown in Figures 4.4 (d) and 4.5(d) respectively.

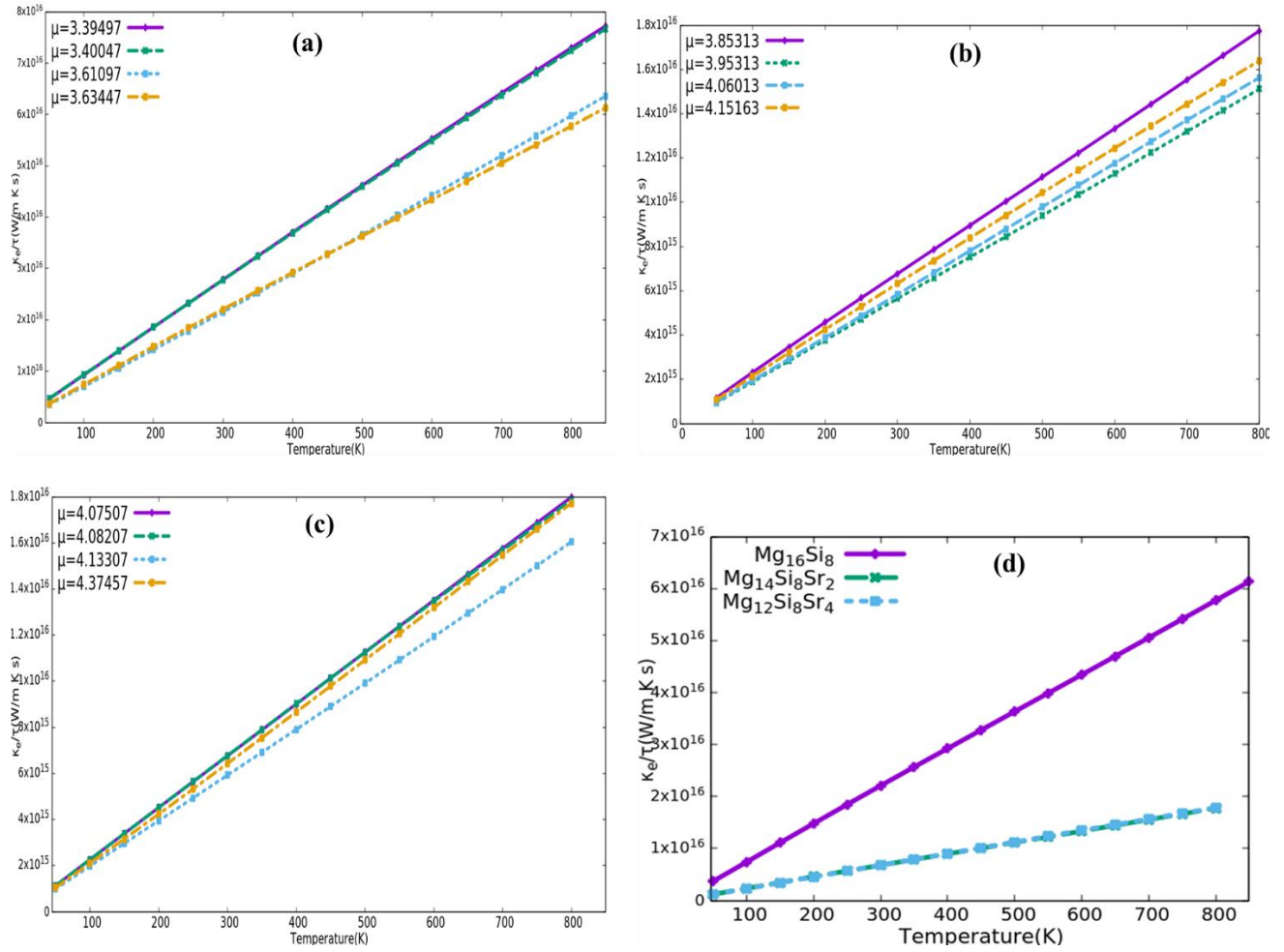


Figure 4.5 Electronic thermal conductivity as a function of temperature and chemical potentials for; (a),  $Mg_{16}Si_8$ , (b)  $Mg_{14}Si_8Sr_2$ , (c)  $Mg_{12}Si_8Sr$ , and (d) Effect of chemical potentials on all compounds respectively

We have also observed as the carrier concentration increases when the concentration of Sr increases. Unlike undoped compounds, the electrical conductivity and electronic thermal conductivity of doped compounds are stable at high temperatures. As shown in Figures 4.7 (d) and 4.6 (d), the continuous increment of electrical conductivity and electronic thermal conductivity of doped compounds with the number of carrier concentrations makes it better for thermoelectric application at higher temperatures. This shows that even though the electrical conductivity and electronic thermal conductivity reduced, due to reduction of carrier mobility as a result of

scattering, these two property continuously increases at a higher temperature for doped compound relative to undoped compound.

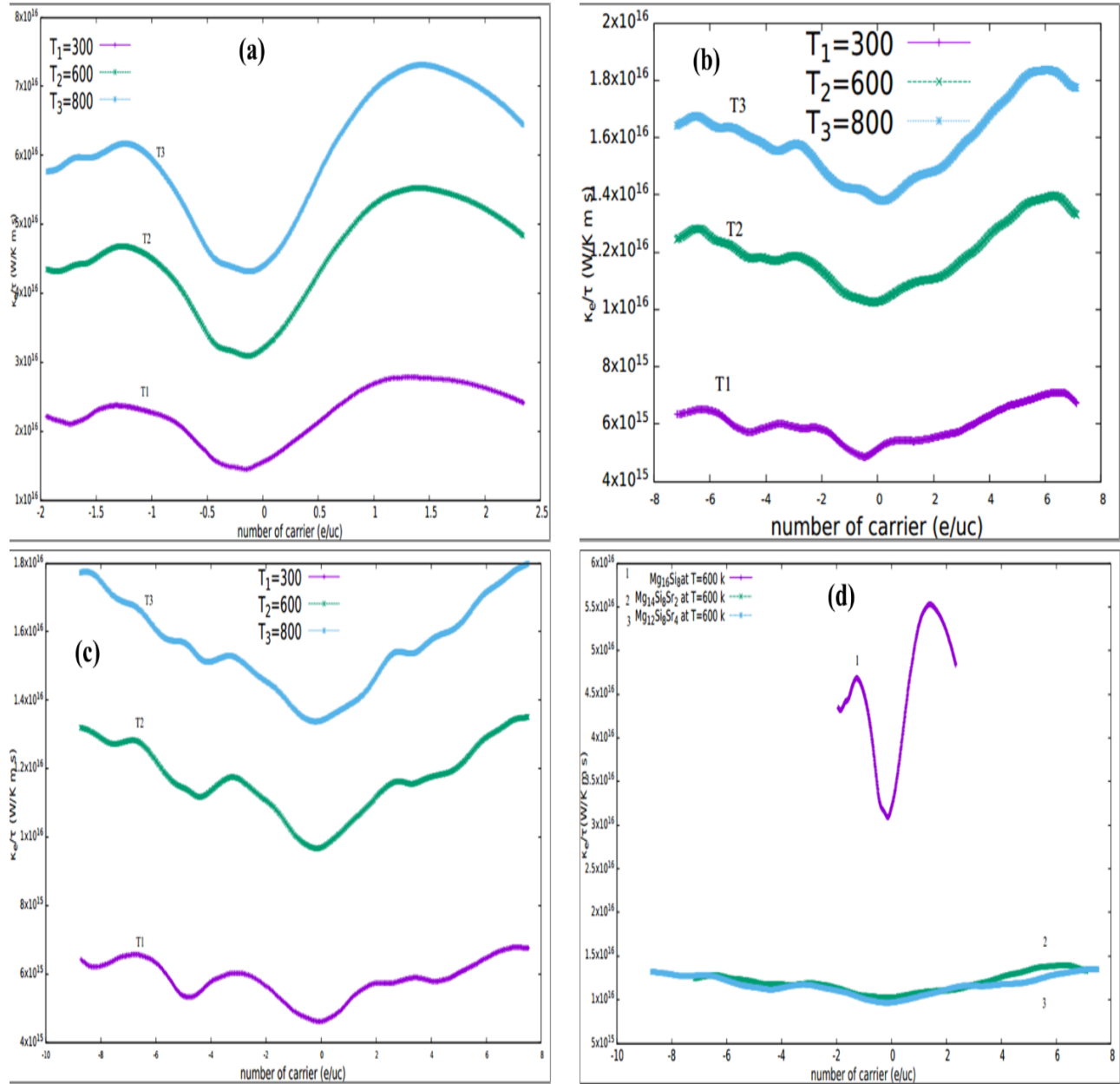


Figure 4.6 Electronic thermal conductivity per-relaxation time for (a),  $\text{Mg}_{16}\text{Si}_8$ , (b)  $\text{Mg}_{14}\text{Si}_8\text{Sr}_2$ , (c)  $\text{Mg}_{12}\text{Si}_8\text{Sr}$ , and (d) comparison of the three as a function of temperature and the number of carriers per unit volume respectively.

At low carrier concentration  $\text{Mg}_{16}\text{Si}_8$  show p-type behavior and n-type behavior while it shifts to n-type at the high number of carrier concentration for all temperatures. The properties do not varied with the temperature at a high number of carrier concentrations. But the variation of electrical

conductivity and electronic thermal conductivity with temperature is shown at the low number of carrier concentrations as shown in Figures 4.7 and 4.6 for all compounds.

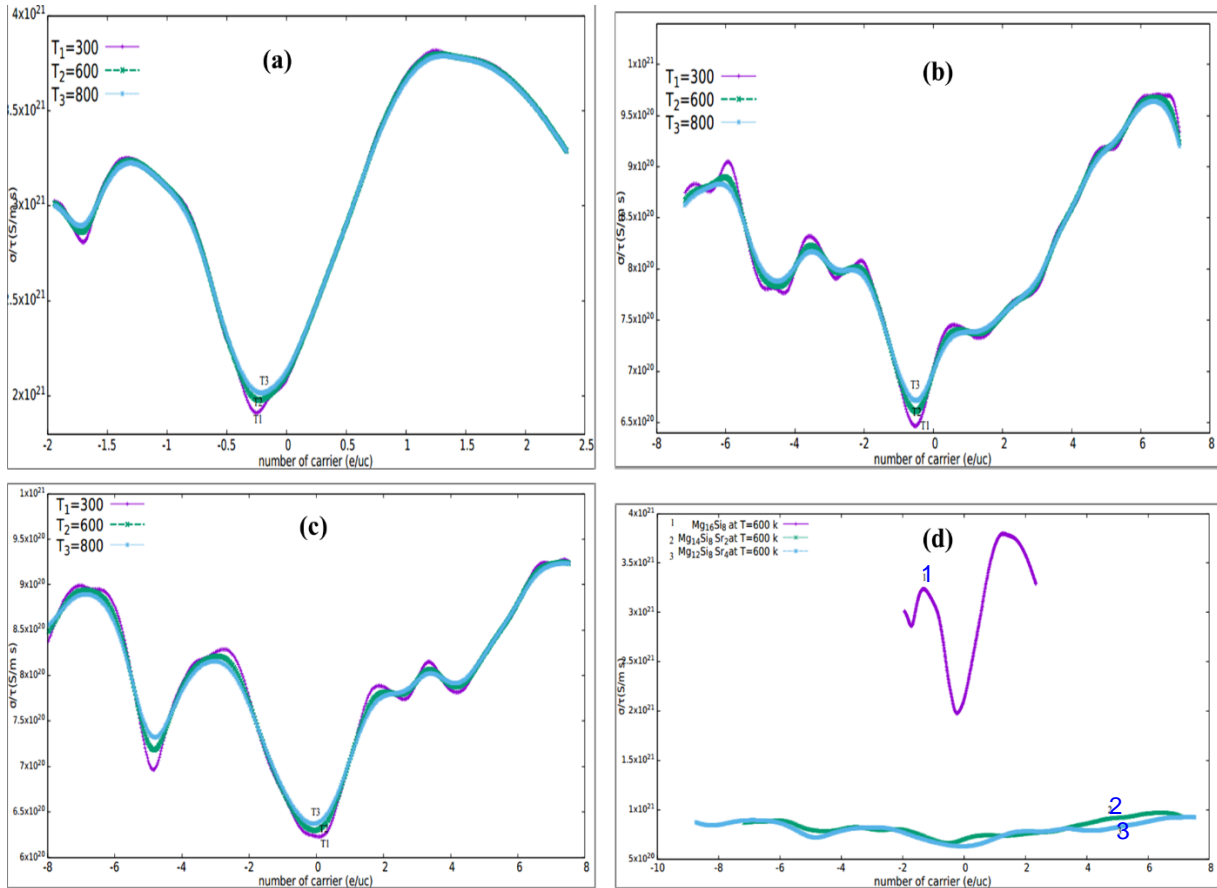


Figure 4.7 Electrical conductivity as a function of temperature and the number of carriers for (a),  $\text{Mg}_{16}\text{Si}_8$ , (b)  $\text{Mg}_{14}\text{Si}_8\text{Sr}_2$ , (c)  $\text{Mg}_{12}\text{Si}_8\text{Sr}$ , and (d) comparison of the three

As shown in Figures 4.3, 4.4, 4.5, 4.7, and 4.8 electronic transport properties were studied as a function of temperature and carrier concentration. The Seebeck effect is independent of relaxation time and the values can be taken as pure values of the Seebeck coefficient. The doped compound has a higher number of carriers of undoped compounds. The Seebeck coefficient increases with increasing temperatures and shows good property for n-type. The graphs show sinusoidal function due to the existence of other factors that affect the properties. The electrical conductivity and electronic thermal conductivity shows the same behaviors as shown in figure 4.4 and 4.5. It

increase with increasing temperature and show reduction behaviors at a large number of carriers. Both of them depend on relaxation time and their net values cannot be acquired without the knowledge of relaxation time. But the approximation may be taken if its value is necessarily needed. It is not an easy task to know the values of electronic transport properties by only describing the number of carrier concentrations, relaxation time, and temperature. It also needs other factors like the chemical potential to define the perfect correlation values with other properties. So in this work, we have also tried to show the effects of chemical potentials on these properties as shown in figure 4.8 by comparing each other as a function of carrier concentration and temperature for both doped and undoped compounds.

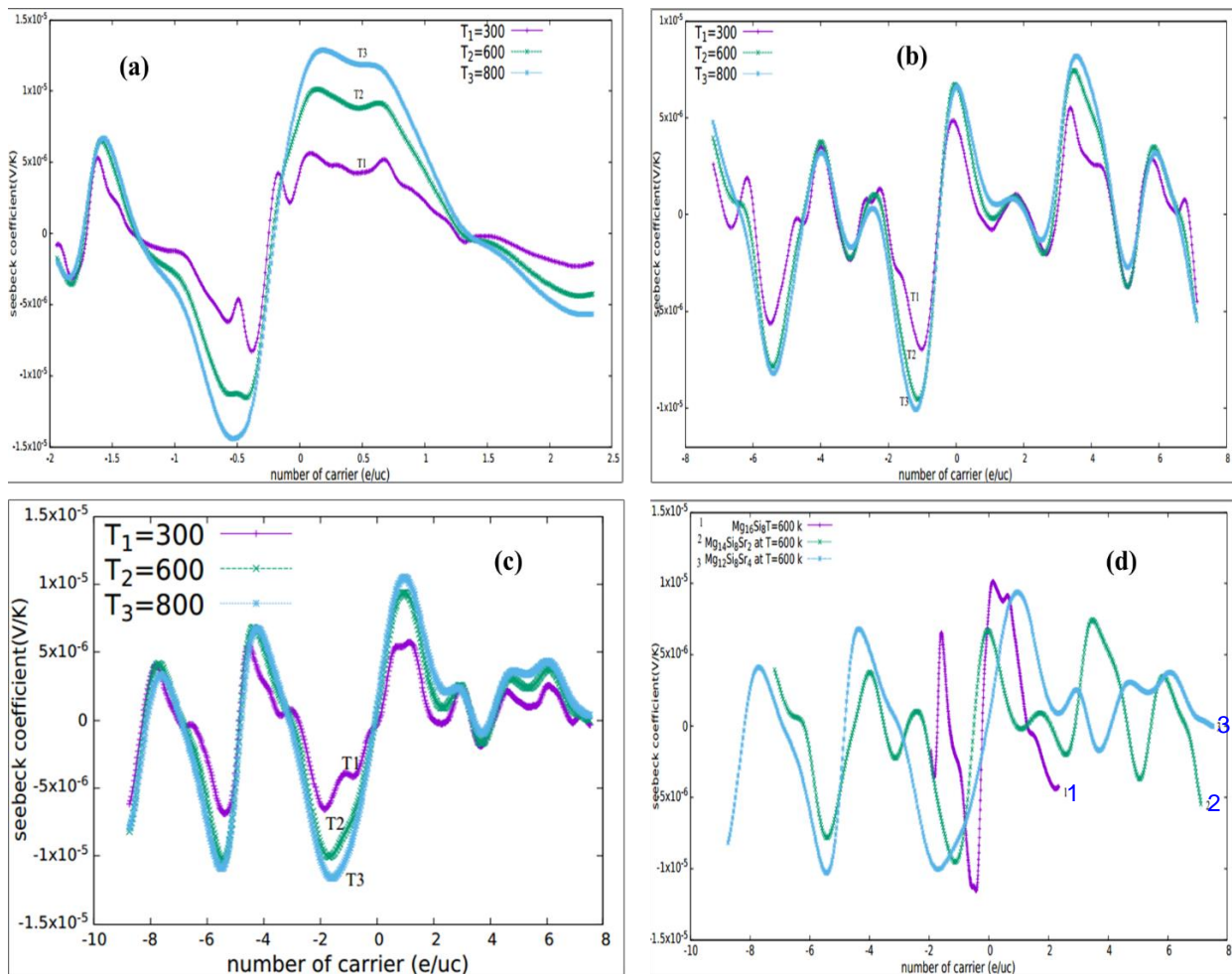


Figure 4.8 Seebeck coefficient as a function of temperature and the number of carriers for (a),  $\text{Mg}_{16}\text{Si}_8$ , (b)  $\text{Mg}_{14}\text{Si}_8\text{Sr}_2$ , (c)  $\text{Mg}_{12}\text{Si}_8\text{Sr}_4$ , and (d) comparison of the three

From all calculation of electronic parts, we can generalize the electronic properties by power factor which is the multiplication of the square of Seebeck with electrical conductivity ( $S^2\sigma$ ). The power factor increases with increasing dopant concentration as shown in figure 4.9. This is due to the increments of Seebeck coefficient in highly doped ( $\text{Mg}_{12}\text{Si}_8\text{Sr}_4$ ) as shown in figure 4.3 (d).

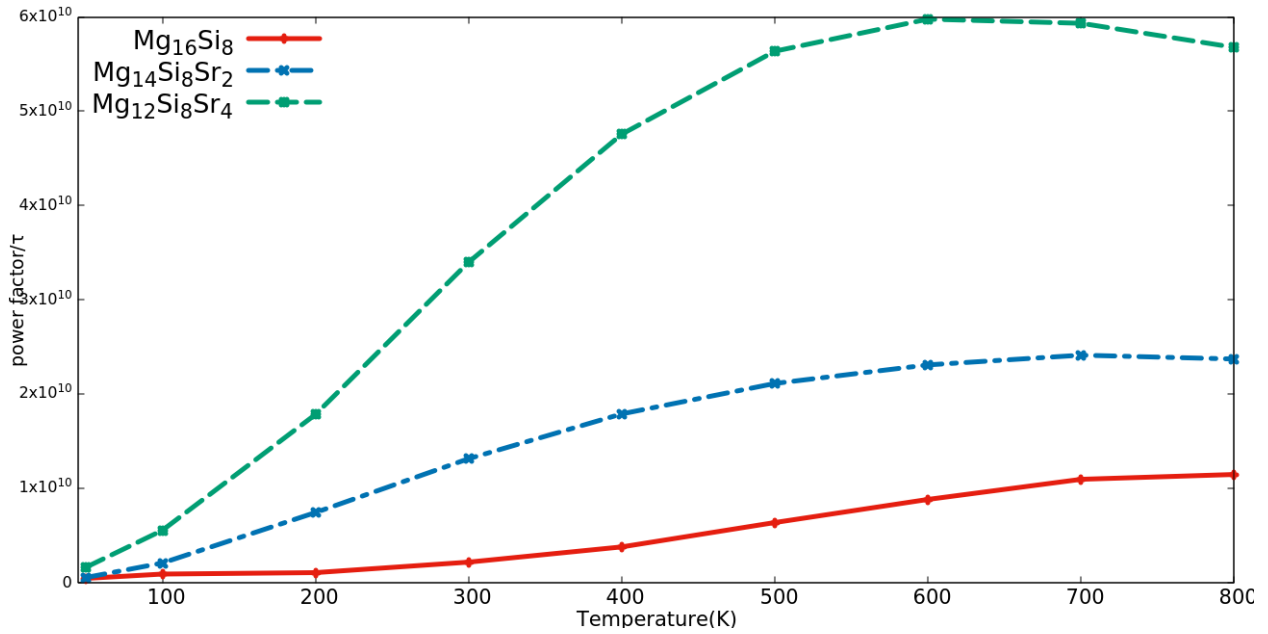


Figure 4.9 Power factor per relaxation time for the three compound ( $\text{Mg}_{16}\text{Si}_8$ ,  $\text{Mg}_{14}\text{Si}_8\text{Sr}_2$ , and  $\text{Mg}_{12}\text{Si}_8\text{Sr}_4$ )

### 4.3 Phonon properties analysis

Before calculating phonon properties we had computed the thermodynamic properties of the unit cell material. This is necessarily needed to compute the Debye temperature at which the phonon vibration is investigated. As shown in figure 4.10 (d) the heat capacity shows nearly constant values above the temperature of 800K. Above this temperature, the phonon vibration of our materials are reaching the ultimate values of vibration and all necessary properties can be studied beyond this temperature. As shown in figure 4.10(a) and b) the phonon density of states and phonon dispersion, which shows the existence of acoustic and optical phonon, are also computed.

The acoustic phonon, which is very important for lattice thermal conductivity examination, is occurred at a relatively low frequency in gamma (G) point in the first Brillouin zone.

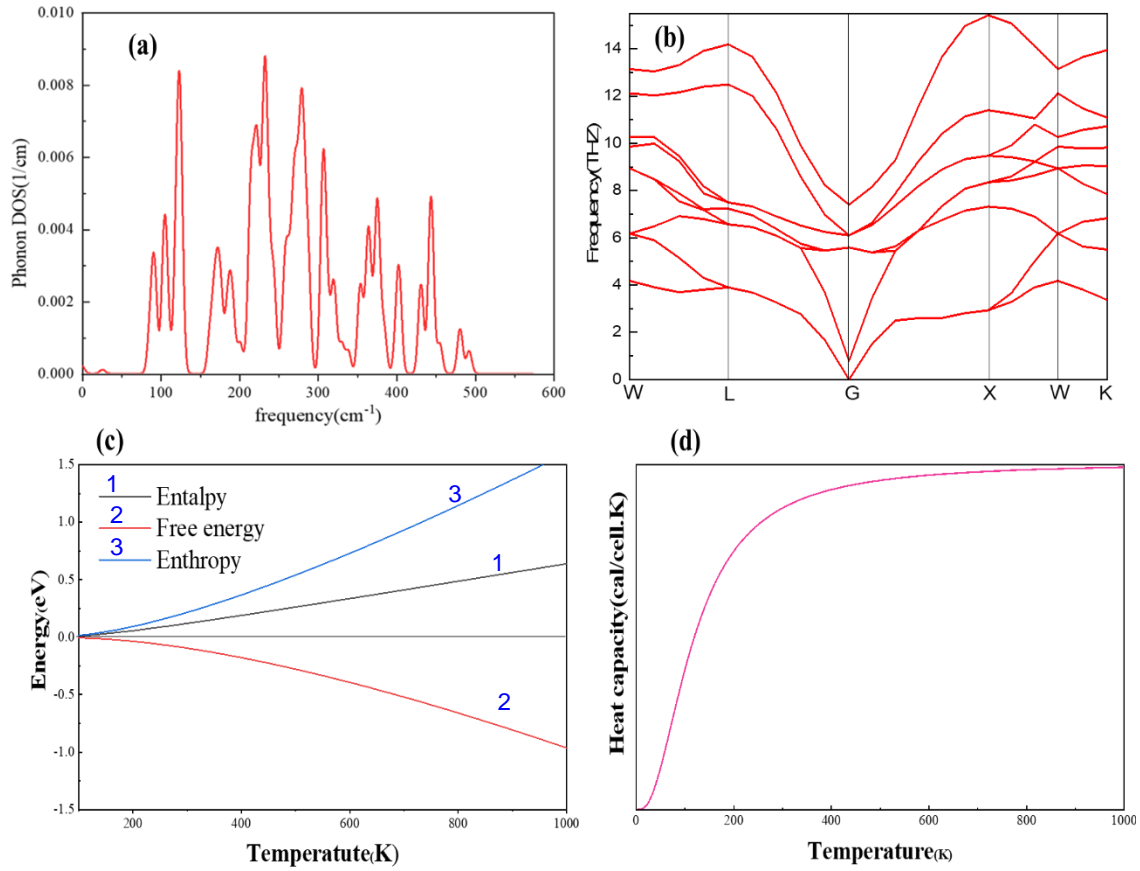


Figure 4.10 Thermodynamic properties of Mg<sub>2</sub>Si

Phonon DOS(a), phonon dispersion(b), Entropy, enthalpy and Gibbs free energy(c), (d) heat capacity

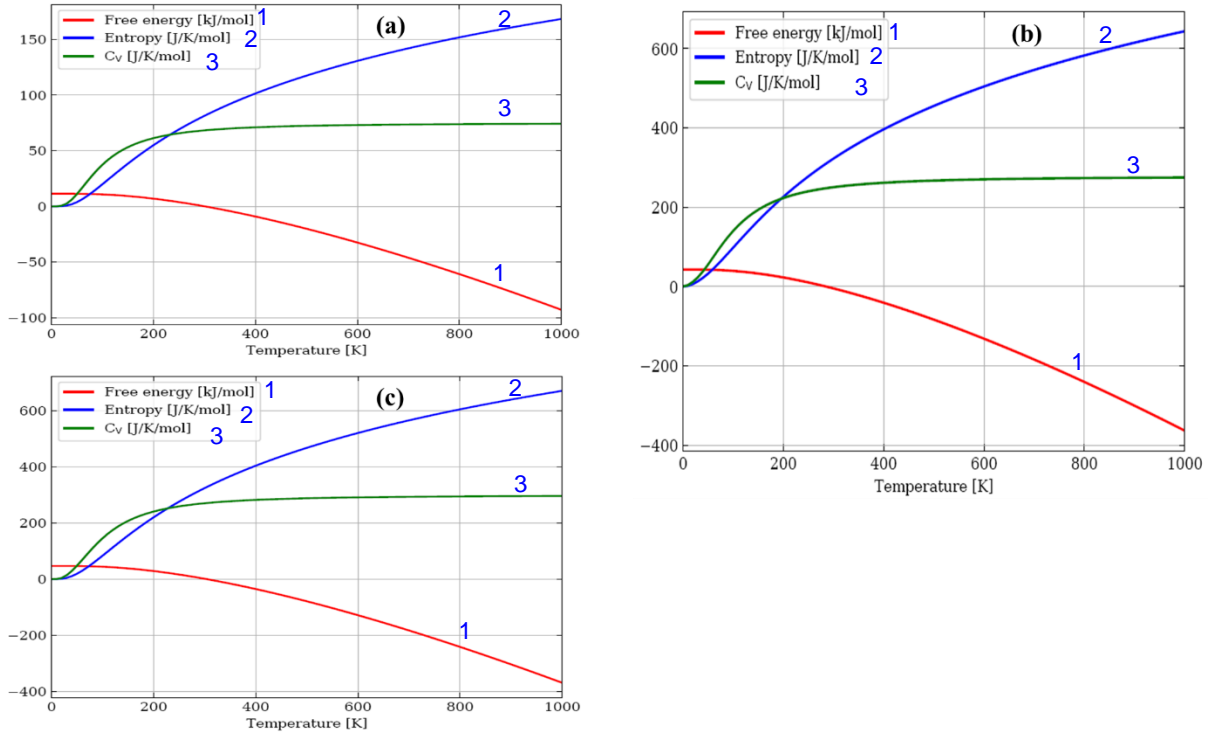


Figure 11 Thermodynamic properties of a)  $\text{Mg}_{16}\text{Si}_8$ , (b)  $\text{Mg}_{14}\text{Si}_8\text{Sr}_2$ , and (c)  $\text{Mg}_{12}\text{Si}_8\text{Sr}_4$

The thermodynamic properties of doped compounds were changed when related to undoped compounds. The entropy, specific heat capacity, and free energy are all increased in both  $\text{Mg}_{14}\text{Si}_8\text{Sr}_2$  and  $\text{Mg}_{12}\text{Si}_8\text{Sr}_4$  as shown in figure 11 (b) and (d) respectively. From graphs of entropy, we understand that the disorder of the crystal system is increased as the concentration of Sr increases. This is due to the higher radius of Sr than Mg which introduces crystal distortion.

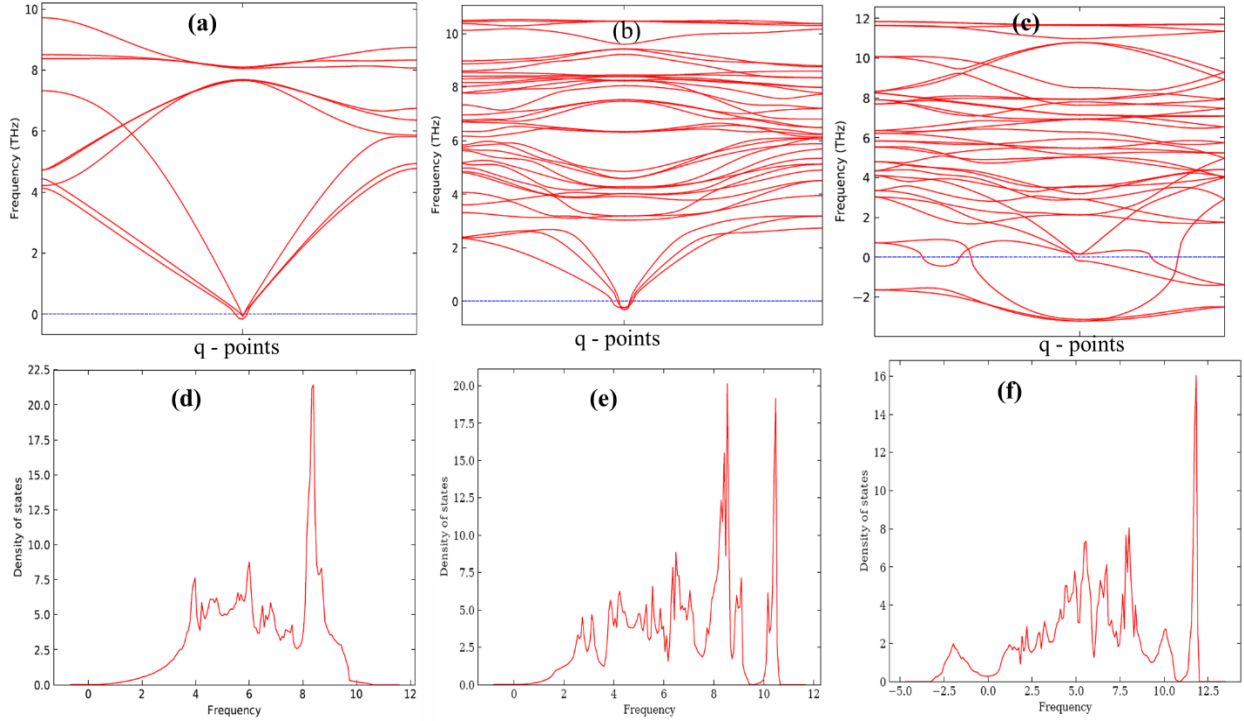


Figure 11 phonon dispersion and phonon DOS of  $\text{Mg}_{16}\text{Si}_8$ (a, d),  $\text{Mg}_{14}\text{Si}_8\text{Sr}_2$ (b, e), and  $\text{Mg}_{12}\text{Si}_8\text{Sr}_4$ (c, f)

As we introduce in the first chapter of this thesis, the lattice thermal conductivity is an important parameter for the good performance of thermoelectric materials. Materials with low thermal conductivity and high power factor can be preferred as the best thermoelectric materials. This characteristic can be acquired by introducing the dopant atom and optimize the other thermoelectric properties as described in the novel approach of the literature reviews in chapter two. This is the method we have used to minimize the lattice thermal conductivity in all of this work. We have used substitutional doping of strontium (Sr) at the magnesium (Mg) site of the  $\text{Mg}_2\text{Si}$  compound. Introducing dopant atoms to the materials creates phonon scattering[59], which minimizes the mean free path. The lattice thermal conductivity is related to the mean free path by the Eq. (15) in Appendix B. phonon scattering time was not calculated in this work.



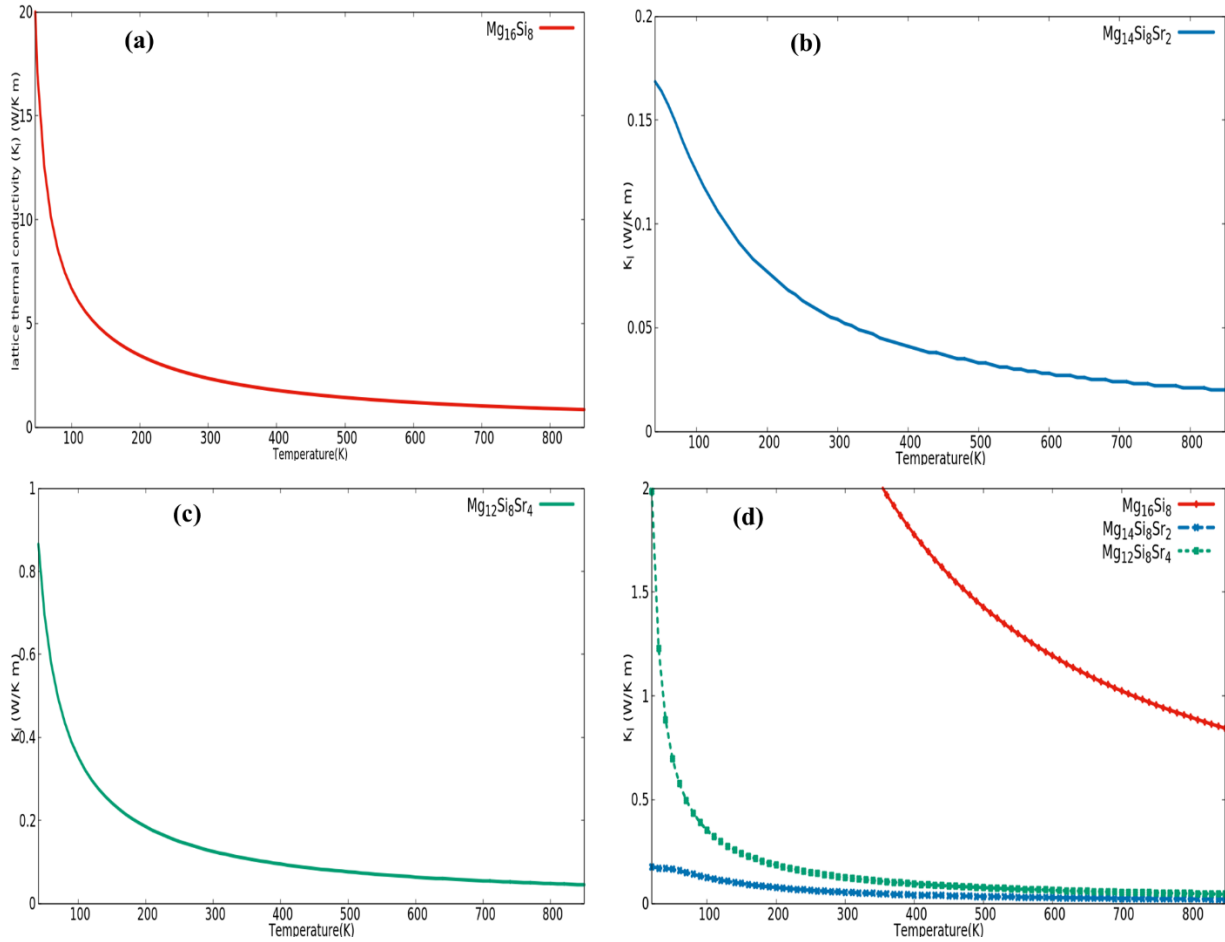


Figure 4.11 Lattice thermal conductivity of a)  $\text{Mg}_{16}\text{Si}_8$ , (b)  $\text{Mg}_{14}\text{Si}_8\text{Sr}_2$ , and (c)  $\text{Mg}_{12}\text{Si}_8\text{Sr}_4$  and all three (d)

From the bandstructure, we understand that doping Sr into the materials minimizes the band energy and creates the formation of more scattering. For  $\text{Mg}_{14}\text{Si}_8\text{Sr}_2$  the band energy minimized and the bandgap increased in a small amount which favors the scattering of electron-phonon interaction as well as the phonon-phonon interaction at the band edges in the Brillouin zone [47, 60, 61]. As a result, the lattice thermal conductivity is minimized by a large value (from 8 W/Km to 0.2 W/K m at low T and from 1 W/K m to 0.02 W/K m at high T) when related to undoped  $\text{Mg}_{16}\text{Si}_8$  as shown in figure 4.10 (a) and (b).

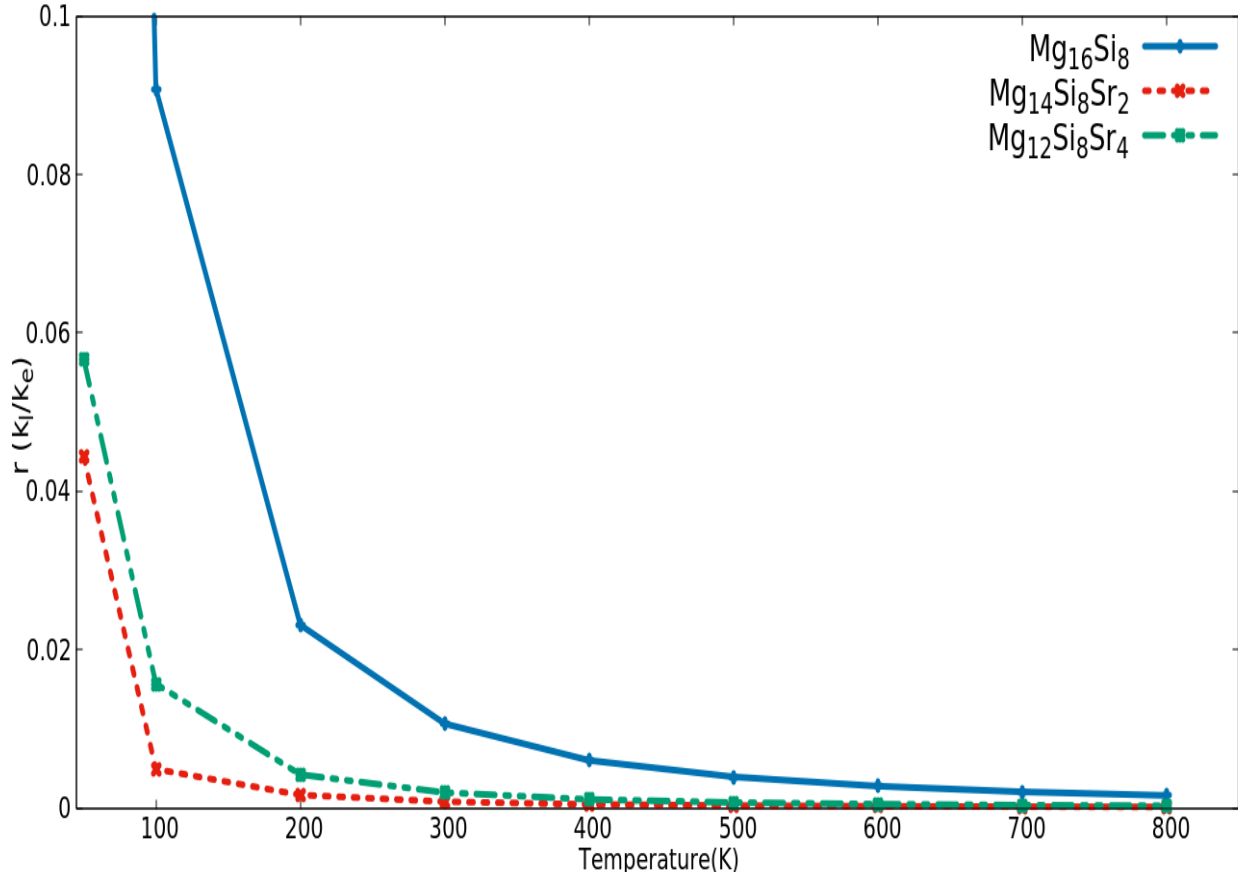


Figure 4.12 The ratio of lattice thermal conductivity to electronic thermal conductivity as a factor of temperature and chemical potential for electronic thermal conductivity.

In this graph, we have estimated the relaxation time as ( $\tau \approx 10^{-14}$  s).

Generally, the efficiency of the thermoelectric material is described by the figure of merit as described in Eq. (3). Let us explain this equation in terms of electronic thermal conductivity and describe our results;

The electrical conductivity and electronic thermal conductivity are the inter-dependent parameters and given by Eq. (13)  $\kappa_e = L\sigma T$  Where  $L = 2.44 \times 10^{-8} \text{ W}\Omega \text{ K}^{-2}$  is Wiedemann–Franz constant.

From this  $\sigma = \frac{\kappa_e}{LT} =$

From this we can get,

$$ZT = \frac{S^2/L}{1 + \frac{k_l}{k_e}}$$

Let ' $r$ ' is the ratio of lattice thermal conductivity to electronic thermal conductivity. So to have a good figure of merit materials must have a large Seebeck coefficient and low ' $r$ '. According to this statement and Eq. (B), Sr doped materials show very good performance than undoped materials as shown in the figure. 11. The doped materials also show a large Seebeck coefficient than undoped materials as shown in figure 4.3(d) for n-type and also the same situation for p-type as shown in figure 4.3 (a), (b), and (c). So the doped materials show better electronic properties and phonon properties when compared to undoped ones.

## 5. CONCLUSION AND RECOMMENDATIONS

Magnesium silicide ( $\text{Mg}_2\text{Si}$ ) is a newly emerged thermoelectric material that is easily available in the earth's crust. Due to its good stability, nontoxicity, and low weight, it is more preferable for thermoelectric material if its properties will have improved. In this work, we have tried to improve its properties by focusing on lattice thermal conductivity by optimizing other properties like the Seebeck effect, electrical conductivity, and electronic thermal conductivity. The computational methods of materials modeling and simulation based on density functional theory (DFT) were fully implemented in this work. Material studio 2017, BoltzTrap code, phonopy, and phono3py are the softwares that were used to evaluate all properties and characteristics of our modeled materials. All the electronic properties and phonon properties were governed by Boltzmann transport equations (BTE). After geometry optimization, the electronic properties and phonon properties were calculated. All properties show a very interesting result even after doping. A very good stable, the optimized electronic properties (figure 4.9), and the much-minimized lattice thermal conductivity (figure 4.11) we got initiate us to report this thesis. We have not seen in any references that the values of lattice thermal conductivity are less than our values in doped  $\text{Mg}_2\text{Si}$ . Generally doping  $\text{Mg}_2\text{Si}$  with strontium (Sr) gives the much-minimized lattice thermal conductivity. We have also seen that a high concentration of strontium (>17 % of the total atom in the unit cell) reduces the bandgap. Finally, recommend that if some improvement will have done on electronic properties, Sr-doped  $\text{Mg}_2\text{Si}$  shows very interesting lattice thermal conductivity for thermoelectric application. The concentration of dopant atoms must be controlled (<17 % is recommended for less lattice thermal conductivity according to our investigation).

## Appendices

### Boltzmann transport equation for Electron solution

The thermoelectric properties calculation is mainly based on the Boltzmann transport theory (BTE), which assumption is based on a distribution function that measures the number of electrons occupation in the neighborhood. The distribution of electrons at thermal equilibrium follows the Fermi-Dirac statistics. To calculate the electronic properties the BoltzTrap code is used to solve the Boltzmann equation by computing all the necessary integrations based on interpolation of a band structure performed or computed with DFT [59]. Therefore all thermoelectric properties are calculated as follows;

The Conductivity tensors  $\sigma_{ij}$  is calculated as;

$$\sigma_{\alpha\beta}(i, k) = e^2 \tau_{i,k} v_{\alpha}(i, k) v_{\beta}(i, k) \quad (1)$$

$$\sigma_{\alpha\beta\gamma}(i, k) = e^2 \tau^2_{i,k} \epsilon_{uv} v_{\alpha}(i, k) v_{\beta}(i, k) M_{\beta u}^{-1} \quad (2)$$

The group velocity and the inverse mass tensor is given by;

$$v_{\alpha}(i, k) = \frac{1 \delta \epsilon_{i,k}}{\hbar \delta k_{\alpha}}, \quad M_{\beta u}^{-1}(i, k) = \frac{1 \delta^2 \epsilon_{i,k}}{\hbar^2 \delta k_{\beta} \delta k_u} \quad (3)$$

The conductivity tensor based on energy ( $\epsilon$ ) in all K-points in Brillouin Zone and all bands is calculated;

$$\sigma_{\alpha\beta}(\epsilon) = \frac{1}{N} \sum_{i,k} \sigma_{\alpha\beta}(i, k) \delta(\epsilon - \epsilon_{i,k}) \quad (4)$$

Where energy  $\epsilon_{(i,k)}$  band index  $i$  and  $k$  vector direction,  $N$  is the number of  $k$ -points

Now if  $g(\varepsilon)$  the density of states,  $n_v$  number of valence electrons per volume,  $f_\mu(T; \varepsilon)$  is the Fermi distribution,  $\Omega$  is the volume of the unit cell,  $e$  the electron charge,  $T$  is temperature, and  $\mu$  is chemical potential or Fermi level, the electrical conductivity ( $\sigma_{ij}$ ), Seebeck coefficient  $S_{ij}$ , electronic thermal conductivity ( $\kappa_{\alpha\beta}^0$ ), and electron or hole carrier concentration  $n(T; \varepsilon)$  is computed by BoltzTrap code as follows;

The conductivity based on the electric field is calculated by;

$$\sigma_{\alpha\beta}(T; \mu) = \frac{1}{\Omega} \int \sigma_{\alpha\beta}(\varepsilon) \left[ -\frac{\delta f_\mu(T; \varepsilon)}{\delta \varepsilon} \right] d\varepsilon \quad (5)$$

The conductivity based on the magnetic field is calculated by;

$$\sigma_{\alpha\beta\gamma}(T; \mu) = \frac{1}{\Omega} \int \sigma_{\alpha\beta\gamma}(\varepsilon) \left[ -\frac{\delta f_\mu(T; \varepsilon)}{\delta \varepsilon} \right] d\varepsilon \quad (6)$$

The conductivity based on the thermal gradient is calculated by;

$$v_{\alpha\beta}(T; \mu) = \frac{1}{eT\Omega} \int \sigma_{\alpha\beta}(\varepsilon - \mu) \left[ -\frac{\delta f_\mu(T; \varepsilon)}{\delta \varepsilon} \right] d\varepsilon \quad (7)$$

The thermal conductivity due to electronic contribution is calculated by;

$$\kappa_{\alpha\beta}^0(T; \mu) = \frac{1}{e^2 T \Omega} \int \sigma_{\alpha\beta}(\varepsilon) (\varepsilon - \mu)^2 \left[ -\frac{\delta f_\mu(T; \varepsilon)}{\delta \varepsilon} \right] d\varepsilon \quad (8)$$

The Seebeck coefficient is calculated by;

$$S_{ij} = E_i (\Delta_j T)^{-1} = (\sigma^{-1})_{\alpha i} v_{\alpha j} \quad (9)$$

The doping carrier concentration is calculated by;

$$n(T; \varepsilon) = n_v - \frac{1}{\Omega} \int g(\varepsilon) f_\mu(T; \varepsilon) d\varepsilon \quad (10)$$

## APPENDIX B

### Boltzmann transport equation for Phonon properties calculation

Every calculation for thermal properties is based on Hamiltonian expansions. It is started from general and defines every parameter one by one. The general Hamiltonian is defined as;

$$H = \Phi_0 + T + H_2 + H_3 + \dots \quad (1)$$

Each parameter in the equations (1) is expressed as follows;

$$T = \frac{1}{2} \sum_{lk\alpha} m_k [u_\alpha(lk)]^2, \quad (2)$$

$$H_2 = \frac{1}{2} \sum_{lk\alpha} \sum_{l'k'\beta} \Phi_{\alpha\beta}(lk, l'k') u_\alpha(lk) u_\beta(l'k'), \quad (3)$$

$$H_3 = \frac{1}{6} \sum_{lk\alpha} \sum_{l'k'\beta} \sum_{l''k''\gamma} \Phi_{\alpha\beta\gamma}(lk, l'k', l''k'') \times u_\alpha(lk) u_\beta(l'k') u_\gamma(l''k''), \quad (4)$$

Where,

$\Phi_0$  - is correspond to the constant potential,

$H_n$  - is n-body crystal potential terms,

T - is kinetic energy,

$\Phi_{\alpha\beta}$  - is the harmonic force constant,

$\Phi_{\alpha\beta\gamma}$  - is an anharmonic cubic force constant

$U_{(lk)}$  - is the atomic displacement of  $k^{th}$  atom in  $l^{th}$  unit cell

m - is the atomic mass of  $k$ -type, and the symbols  $\alpha$ ,  $\beta$ , and  $\gamma$  are represented the Cartesian indices.

According to the user guides of phono3py and phonopy and many references [59, 60, 62-65], the harmonic Hamiltonian  $H$  is defined by;

$$H = H_2 + T \quad (5)$$

The atomic displacement is given by;

$$u_\alpha = \left( \frac{\hbar}{2Nm_k} \right)^{\frac{1}{2}} \sum_{qj} \omega_{qj}^{-\frac{1}{2}} [\tilde{\alpha} + \tilde{\alpha}^\dagger_{-qj}] e^{iq \cdot r(lk)} W_\alpha(k, qj) \quad (6)$$

Where  $\hbar$  is the reduced Planck constant,  $N$  is the number of unit cells in the crystal,  $\omega$  is harmonic frequency,  $W_\alpha(qj)$  polarization vector,  $\tilde{\alpha}$ , and  $\tilde{\alpha}^\dagger$  are the phonon creation and annihilation operators of the wave vector  $q$  and normal mode of band index  $j$ , and  $r(lk)$  is the equilibrium atomic position. The polarization vector  $W_\alpha(qj)$  and is harmonic frequency  $\omega(qj)$  are obtained from the eigenvalue problem of a dynamical matrix  $D(q)$  as follows;

$$\sum_{k'\beta} D_{\alpha\beta}(kk', q) W_\beta(k', qj) = \omega_{qj}^2 W_{\alpha j}(k, qj) \quad (7)$$

$$D_{\alpha\beta}(kk', q) = \frac{1}{\sqrt{m_k m_{k'}}} \sum_{l'} \Phi_{\alpha\beta}(0k, l'k') e^{iq \cdot [r(l'k') - r(0k)]} \quad (8)$$

Using Eq. (6) we can easily express Hamiltonian for both harmonic ( $H_2$ ) and anharmonic ( $H_3$ ) as shown in Eq. (9) and (10). The harmonic part is expressed as the sum of harmonic oscillators,

$$H_2 = \sum_{qj} \hbar \omega_{qj} \left( \frac{1}{2} + \tilde{\alpha}_{qj}^\dagger \tilde{\alpha}_{qj} \right) \quad (9)$$

The anharmonic part is expressed as a sum of three phonon collisions,

$$H_3 = \sum_{\lambda\lambda'\lambda''} \Phi_{\lambda\lambda'\lambda''} (\tilde{\alpha}_\lambda + \tilde{\alpha}_{-\lambda}^\dagger) ((\tilde{\alpha}_{\lambda'} + \tilde{\alpha}_{-\lambda'}^\dagger) (\tilde{\alpha}_{\lambda''} + \tilde{\alpha}_{-\lambda''}^\dagger)) \quad (10)$$



Where  $\Phi_{(\lambda\lambda'\lambda'')}$  is given as;

$$\begin{aligned}\Phi_{\lambda\lambda'\lambda''} &= \frac{1}{\sqrt{N}} \frac{1}{3!} \sum_{kk'k''} \sum_{\alpha\beta\gamma} W_{\alpha}(\kappa, \lambda) W_{\beta}(\kappa', \lambda') W_{\gamma}(\kappa'', \lambda'') \sqrt{\frac{\hbar}{2m_{\kappa}\omega_{\lambda}}} \sqrt{\frac{\hbar}{2m_{\kappa'}\omega_{\lambda'}}} \sqrt{\frac{\hbar}{2m_{\kappa''}\omega_{\lambda''}}} \\ &\times \sum_{ll'} \Phi_{\alpha\beta\gamma}(0k, l'k'l''k'') e^{iq'.[r(l'k')-r(0k)]} e^{iq''.[r(l''k'')-r(0k)]} \\ &\times e^{i(q+q'+q'')-r(0k)} \Delta(q + q' + q'')\end{aligned}\quad (11)$$

### Phonon lifetime calculation

The Relaxation Time Approximation (RTA) solves the problems non-diagonal form of the collision. The solution is performed by assuming the rate at which a phonon wave vector ( $\mathbf{q}$ ) relaxes does not depend on the non-equilibrium situation of the phonons colliding with it. Phonon lifetime is calculated from imaginary self-energy. Assume if the imaginary part of self-energy is represented by,  $\Gamma_{\lambda}(\omega_{\lambda})$

$$\Gamma_{\lambda}(\omega) = \frac{18\pi}{\hbar^2} \sum_{\lambda'\lambda''} |\phi_{-\lambda\lambda'\lambda''}|^2 \{ (n_{\lambda'} + n_{\lambda''} + 1) \delta(\omega - \omega_{\lambda'} - \omega_{\lambda''}) + (n_{\lambda'} - n_{\lambda''}) [\delta(\omega + \omega_{\lambda'} - \omega_{\lambda''}) - \delta(\omega - \omega_{\lambda'} + \omega_{\lambda''})] \} \quad (12)$$

Where  $\lambda$  phonon mode,  $\phi_{-\lambda\lambda'\lambda''}$  constant potentials,  $\omega$  frequency and  $n_{\lambda'}$  is the phonon occupation number and give by;

$$n_{\lambda'} = [\exp\left(\frac{\hbar\omega_{\lambda'}}{K_B T}\right) - 1]^{-1} \quad (13)$$

Now the relaxation time is given by;

$$\tau_{\lambda} = \frac{1}{\Gamma_{\lambda}(\omega_{\lambda})} \quad (14)$$

### Lattice thermal conductivity calculation

In the Boltzmann transport equation, the lattice thermal conductivity  $\kappa$  is calculated based on relaxation time (RTA) as follows;

$$\kappa = \frac{1}{NV_0} \sum_{\lambda} C_{\lambda} v_{\lambda} \otimes v_{\lambda} \tau_{\lambda} \quad (15)$$

where  $N$  is the number of unit cells in the system,  $V_0$  of the volume of the unit cell, the symbol  $\lambda$  represents the phonon mode as the pair of phonon wave vector  $q$ ,  $v_\lambda$  is group velocity and  $C_\lambda$  is the mode heat capacity which given as;

$$C_\lambda = K_B \left( \frac{\hbar\omega_\lambda}{K_B T} \right)^2 \frac{\exp\left(\frac{\hbar\omega_\lambda}{K_B T}\right)}{\left[\exp\left(\frac{\hbar\omega_\lambda}{K_B T}\right) - 1\right]^2} \quad (16)$$

Where  $\omega_\lambda = \omega(q,j)$  is the phonon frequency,  $T$  is the temperature, and  $k_B$  denote the reduced Planck constant the group velocity is calculated as;

$$v_\alpha(\lambda) \equiv \frac{\delta \omega_\lambda}{\delta q_\alpha} \quad (17)$$

$$= \frac{1}{2\omega_\lambda} \sum_{\kappa\kappa'\beta\gamma} W_\beta(\kappa, \lambda) \frac{\delta D_{\beta\gamma}(\kappa\kappa', q)}{\delta q_\alpha} W_\gamma(\kappa', \lambda) \quad (18)$$

## REFERENCES

1. Sharma, Sonu and Sudhir K. Pandey, A first principle study of electronic band structures and effective mass tensors of thermoelectric materials: PbTe, Mg<sub>2</sub>Si, FeGa<sub>3</sub>, and CoSb<sub>3</sub>. Computational Materials Science, 2014. **85**: p. 340-346.
2. M. Einhorn, B. A. D. Williamson and D. O. Scanlon, Computational prediction of the thermoelectric performance of LaZnOPn (Pn = P, As). Journal of Materials Chemistry A, 2020. **8**(16): p. 7914-7924.
3. J. Julio Gutiérrez Moreno, Jiang Cao, Marco Fronzi & M. Hussein N. Assadi, A review of recent progress in thermoelectric materials through computational methods. Materials for Renewable and Sustainable Energy, 2020. **9**(3): p. 16.
4. Zhang, Y.Z., Y.H. Han, and Q.S. Meng, The performance of Mg<sub>2</sub>Si-based thermoelectric materials prepared from MgH<sub>2</sub>. Materials Research Innovations, 2015. **19**(sup1): p. S1-264-S1-268.
5. Sharma, S. and U. Schwingenschlögl, Thermoelectric Response in Single Quintuple Layer Bi<sub>2</sub>Te<sub>3</sub>. ACS Energy Letters, 2016. **1**(4): p. 875-879.
6. Alam, H. and S. Ramakrishna, A review on the enhancement of figure of merit from bulk to nano-thermoelectric materials. Nano Energy, 2013. **2**(2): p. 190-212.
7. Kato, T., Y. Sago, and H. Fujiwara, J. Appl. Phys., 2011. **110**.
8. Madelung, O., Semiconductors: data handbook. 2004, Berlin: Springer.
9. Xiaoli Liu, Ruchita Jani, Esther Orisakwe, Conrad Johnston, Piotr Chudzinski, Ming Qu\*, Brian Norton, Niall Holmes, Jorge Kohanoff, Lorenzo Stella, Hongxi Yin, Kazuaki Yazawa, State of the art in composition, fabrication, characterization, and modeling methods of cement-based thermoelectric materials for low-temperature applications. Renewable and Sustainable Energy Reviews, 2020: p. 110361.
10. Balout, H., P. Boulet, and M.-C. Record, Thermoelectric Properties of Mg<sub>2</sub>Si Thin Films by Computational Approaches. The Journal of Physical Chemistry C, 2014. **118**(34): p. 19635-19645.
11. Samson Shittu<sup>a</sup> Guiqiang Li<sup>a</sup> Xudong Zhao<sup>a</sup> Xiaoli Ma<sup>a</sup> Yousef Golizadeh Akhlaghi<sup>a</sup> Emmanuel Ayodele<sup>b</sup>, High performance and thermal stress analysis of a segmented annular thermoelectric generator. Energy Conversion and Management, 2019. **184**: p. 180-193.

12. Hashibon, A., First-principles density functional theory study of native point defects in Bi<sub>2</sub>Te<sub>3</sub>. *Phys. Rev. B*, 2011. **84**.
13. Kolezynski, A., P. Nieroda, and K.T. Wojciechowski, Li doped Mg<sub>2</sub>Si p-type thermoelectric material: Theoretical and experimental study. *Computational Materials Science*, 2015. **100**: p. 84-88.
14. M. S. Dresselhaus, G. Chen, M. Y. Tang, R. G. Yang, H. Lee, D. Z. Wang, Z. F. Ren, J.-P. Fleurial, P. Gogna, *New Directions for Low-Dimensional Thermoelectric Materials*. *Advanced Materials*, 2007. **19**: p. 1043-1053.
15. H. Udono, Y. Yamanaka, M. Uchikoshi, and M. Isshiki, *J. Phys. Chem. Solids* 74, 311 (2013).
16. Masayasu Akasaka<sup>a,b</sup> Tsutomu Iida<sup>a</sup> Yoshifumi Takanashi<sup>a</sup>, *Thin Solid Films*, 2007. **515**.
17. M. W. Oha), J. H. Son, B. S. Kim, S. D. Park, B. K. Min, and H. W. Lee, Antisite defects in n-type Bi<sub>2</sub>(Te,Se)<sub>3</sub>: Experimental and theoretical studies. *Journal of Applied Physics*, 2014. **115**(13): p. 133706.
18. Amin Nozariasbmarz<sup>1,2</sup>, Palash Roy<sup>3</sup>, Zahra Zamanipour<sup>3</sup>, J. Houston Dycus<sup>2</sup>, Matthew J. Cabra<sup>1,2</sup>, James M. LeBeau<sup>2</sup>, Jerzy S. Krasinski<sup>3</sup>, and Daryoosh Vashaee<sup>1,2,a</sup>), Comparison of thermoelectric properties of nanostructured Mg<sub>2</sub>Si, FeSi<sub>2</sub>, SiGe, and nanocomposites of SiGe–Mg<sub>2</sub>Si, SiGe–FeSi<sub>2</sub>. *APL Materials*, 2016. **4**(10): p. 104814.
19. Airan Li,<sup>1</sup> Chenguang Fu<sup>2</sup>, Xinbing Zhao<sup>1</sup> and Tiejun Zhu <sup>1</sup>, High-Performance Mg<sub>3</sub>Sb<sub>2</sub>-Bi Thermoelectrics: Progress and Perspective. *Research*, 2020. **2020**: p. 1934848.
20. de Boor, J., A. Berche, and P. Jund, Density of States Effective Mass for p-Type Mg<sub>2</sub>Si–Mg<sub>2</sub>Sn Solid Solutions: Comparison between Experiments and First-Principles Calculations. *The Journal of Physical Chemistry C*, 2020. **124**(28): p. 14987-14996.
21. Kei Hayashi<sup>1,a</sup>), Wataru Saito<sup>1</sup>, Kazuya Sugimoto<sup>2</sup>, Kenji Ohoyama<sup>2</sup>, Kouichi Hayashi<sup>3,4</sup>, Naohisa Happo<sup>5</sup>, Masahide Harada<sup>6</sup>, Kenichi Oikawa<sup>6</sup>, Yasuhiro Inamura<sup>6</sup>, and Yuzuru Miyazaki<sup>1</sup>, Preparation, thermoelectric properties, and crystal structure of boron-doped Mg<sub>2</sub>Si single crystals. *AIP Advances*, 2020. **10**(3): p. 035115.
22. Nader Farahi, ORCID logo <sup>\*a</sup> Christian Stiewe,<sup>a</sup> D. Y. Nhi Truong,<sup>a</sup> Johannes de Boor ORCID logo <sup>a</sup> and Eckhard Müller<sup>ab</sup> ), High-efficiency Mg<sub>2</sub>(Si, Sn)-based thermoelectric materials: scale-up synthesis, functional homogeneity, and thermal stability. *RSC Advances*, 2019. **9**(40): p. 23021-23028.

23. Yingmin Li<sup>1</sup>, Tianyu Ma<sup>1</sup>, Yuyan Ren<sup>2</sup>, Tongyu Liu<sup>1</sup> and Xue Zou<sup>1</sup>, First-principles calculation on the structure stability, elastic properties and electronic structure of P-doped Mg<sub>2</sub>Si. *Materials Research Express*, 2020. **7**(3): p. 036533.
24. Argaman, N. and G. Makov, *Density Functional Theory -- an introduction*. American Journal of Physics, 1998. **68**.
25. Philip J. Hasnip, Keith Refson, Matt I. J. Probert, Jonathan R. Yates, Stewart J. Clark and Chris J. Pickard, Density functional theory in the solid-state. *Philosophical Transactions of the Royal Society A: Mathematical, Physical and Engineering Sciences*, 2014. **372**(2011): p. 20130270.
26. Argaman, N. and G. Makov, *Density functional theory: An introduction*. American Journal of Physics, 1999. **68**(1): p. 69-79.
27. Bagayoko, D., *Understanding density functional theory (DFT) and completing it in practice*. AIP Advances, 2014. **4**(12): p. 127104.
28. Jones, R.O., *Density functional theory: Its origins, rise to prominence, and future*. *Reviews of Modern Physics*, 2015. **87**(3): p. 897-923.
29. Perdew, J.P. and A. Zunger, Self-interaction correction to density-functional approximations for many-electron systems. *Physical Review B*, 1981. **23**(10): p. 5048-5079.
30. Xuan, F., J.-D. Chai, and H. Su, Local Density Approximation for the Short-Range Exchange Free Energy Functional. *ACS Omega*, 2019. **4**(4): p. 7675-7683.
31. Samsonidze, G. and B. Kozinsky, Accelerated Screening of Thermoelectric Materials by First-Principles Computations of Electron-Phonon Scattering. *Advanced Energy Materials*, 2018. **8**(20): p. 1800246.
32. Yintu Liu,<sup>a</sup> Hanhui Xie,<sup>a</sup> Chenguang Fu,<sup>a</sup> G. Jeffrey Snyder,<sup>\*b</sup> Xinbing Zhao<sup>a</sup> and Tiejun Zhu<sup>\*a</sup>, Demonstration of a phonon-glass electron-crystal strategy in (Hf, Zr)NiSn half-Heusler thermoelectric materials by alloying. *Journal of Materials Chemistry A*, 2015. **3**(45): p. 22716-22722.
33. Yee Kan Koh<sup>1, a)</sup>, C. J. Vineis<sup>2,3</sup>, S. D. Calawa<sup>2</sup>, M. P. Walsh<sup>2</sup>, and David G. Cahill<sup>1</sup>, Lattice thermal conductivity of nanostructured thermoelectric materials based on PbTe. *Applied Physics Letters*, 2009. **94**(15): p. 153101.

34. Liu, Z., et al., Mechanical properties of nanostructured thermoelectric materials  $\alpha$ -MgAgSb. *Scripta Materialia*, 2017. **127**: p. 72-75.
35. Kaur, K., S. Dhiman, and R. Kumar, Strain engineering on the thermoelectric performance of Mg<sub>2</sub>Si. *Materials Research Express*, 2017. **4**(7): p. 075509.
36. Hirayama, N., Y. Imai, and N. Hamada, Conduction band engineering of Mg<sub>2</sub>Si by isotropic strain for enhancement of thermoelectric performance: A first-principles study. *Journal of Applied Physics*, 2020. **127**(20): p. 205107.
37. Wunderlich, W. and M. Amano, Electronic band-structure calculations of Ba<sub>8</sub>Me<sub>x</sub>Si<sub>46-x</sub> clathrates with Me = Mg, Pd, Ni, Au, Ag, Cu, Zn, Al, Sn. *Journal of Electronic Materials*, 2013. **42**: p. s11664-013.
38. Zihang Liu<sup>1,2</sup>, Weihong Gao<sup>1</sup>, Xianfu Meng<sup>1</sup>, Xiaobo Li<sup>1</sup>, Jun Mao<sup>2,3</sup>, Yumei Wang<sup>2,4</sup>, Jing Shuai<sup>2</sup>, Wei Cai<sup>1</sup>, Zhifeng Ren<sup>2\*</sup>, and Jiehe Sui<sup>1\*</sup>, First-Principles and Experimental Studies of Y-Doped Mg<sub>2</sub>Si Prepared Using Field-Activated Pressure-Assisted Synthesis. *Journal of Electronic Materials*, 2011. **40**(5): p. 1209-1214.
39. Hayato Nakasawa, Kei Hayashi, Tomohisa Takamatsu, and Yuzuru Miyazaki, Lattice dynamics and lattice thermal conductivity of CrSi<sub>2</sub> calculated from first principles and the phonon Boltzmann transport equation. *Journal of Applied Physics*, 2019. **126**(2): p. 025105.
40. Fang, T., X. Zhao, and T. Zhu, Band Structures and Transport Properties of High-Performance Half-Heusler Thermoelectric Materials by First Principles. *Materials*, 2018. **11**(5).
41. Jinfeng Yang<sup>a</sup>, Jingyu Li<sup>a</sup>, Chi Zhang<sup>b</sup>, Zhenzhen Feng<sup>a</sup>, Beibei Shi<sup>a</sup>, Wenya Zhai<sup>a</sup>, Yuli Yan<sup>a,\*</sup>, Yuanxu Wang<sup>a,\*\*</sup>, Excellent thermoelectric performance of BaMgSi driven by low lattice thermal conductivity: A promising thermoelectric material. *Journal of Alloys and Compounds*, 2020. **827**: p. 154342.
42. Szczech, J.R., J.M. Higgins, and S. Jin, Enhancement of the thermoelectric properties in nanoscale and nanostructured materials. *Journal of Materials Chemistry*, 2011. **21**(12): p. 4037-4055.
43. Morinaga, M., 11 - Local Lattice Strains Around Alloying Elements in Metals, in *A Quantum Approach to Alloy Design*, M. Morinaga, Editor. 2019, Elsevier. p. 221-260.

44. Hay, B., A brief history of the thermal properties metrology. *Measurement*, 2020. **155**: p. 107556.
45. H.Ihou-Mouko<sup>a</sup>, C.Mercier<sup>a</sup>, J.Tobola<sup>b</sup>, G.Pont<sup>c</sup>, H.Scherrer<sup>a</sup>, Thermoelectric properties and electronic structure of p-type Mg<sub>2</sub>Si and Mg<sub>2</sub>Si<sub>0.6</sub>Ge<sub>0.4</sub> compounds doped with Ga. *Journal of Alloys and Compounds*, 2011. **509**(23): p. 6503-6508.
46. Gorai, P., E.S. Toberer, and V. Stevanović, Computational identification of promising thermoelectric materials among known quasi-2D binary compounds. *Journal of Materials Chemistry A*, 2016. **4**(28): p. 11110-11116.
47. Fang, T., X. Zhao, and T. Zhu, Band Structures and Transport Properties of High-Performance Half-Heusler Thermoelectric Materials by First Principles. *Materials (Basel, Switzerland)*, 2018. **11**(5): p. 847.
48. Chenguang Fu<sup>1</sup>, Shengqiang Bai<sup>2</sup>, Yintu Liu<sup>1</sup>, Yunshan Tang<sup>2</sup>, Lidong Chen<sup>2</sup>, Xinbing Zhao<sup>1,3</sup> & Tiejun Zhu<sup>1,3</sup>, Realizing high figure of merit in heavy-band p-type half-Heusler thermoelectric materials. *Nature Communications*, 2015. **6**(1): p. 8144.
49. Poon, S.J., Recent Advances in Thermoelectric Performance of Half-Heusler Compounds. *Metals*, 2018. **8**(12).
50. Hidetoshi Miyazaki<sup>1\*</sup>, Osman Murat Ozkendir<sup>2,3\*</sup>, Selen Gunaydin<sup>3</sup>, Kosuke Watanabe<sup>1</sup>, Kazuo Soda<sup>4,5,6</sup> & Yoichi Nishino<sup>1</sup>, Probing local distortion around structural defects in half-Heusler thermoelectric NiZrSn alloy. *Scientific reports*, 2020. **10**(1): p. 19820-19820.
51. Karol Synoradzki<sup>1,\*</sup>, Kamil Ciesielski<sup>1</sup>, Igor Veremchuk<sup>2</sup>, Horst Borrmann<sup>2</sup>, Przemysław Skokowski<sup>3</sup>, Damian Szymański<sup>1</sup>, Yuri Grin<sup>2</sup> and Dariusz Kaczorowski<sup>1</sup>, Thermal and Electronic Transport Properties of the Half-Heusler Phase ScNiSb. *Materials (Basel, Switzerland)*, 2019. **12**(10): p. 1723.
52. LaBotz, R.J., D.R. Mason, and D.F. O'Kane, The Thermoelectric Properties of Mixed Crystals of Mg<sub>2</sub>Ge<sub>x</sub>Si<sub>1-x</sub>. *Journal of The Electrochemical Society*, 1963. **110**(2): p. 127.
53. Núñez-Valdez, M., et al., Efficient technique for computational design of thermoelectric materials. *Computer Physics Communications*, 2018. **222**: p. 152-157.
54. Pichanusakorn, P. and P. Bandaru, Nanostructured thermoelectrics. *Materials Science and Engineering: R: Reports*, 2010. **67**(2): p. 19-63.
55. Wang, H., W. Chu, and H. Jin, Theoretical study on thermoelectric properties of Mg<sub>2</sub>Si and comparison to experiments. *Computational Materials Science*, 2012. **60**: p. 224-230.

56. Wei Liu, Xiaojian Tan, Kang Yin, Huijun Liu, Xinfeng Tang, Jing Shi, Qingjie Zhang, and Ctirad Uher, Convergence of Conduction Bands as a Means of Enhancing Thermoelectric Performance of n-Type  $\text{Mg}_2\text{Si}_{1-x}\text{Sn}_x$  Solid Solutions. *Physical Review Letters*, 2012. **108**(16): p. 166601.
57. Philippe Jund<sup>1</sup>, Romain Viennois<sup>1</sup>, Catherine Colinet<sup>2</sup>, Gilles Hug<sup>3</sup>, Mathieu Fèvre<sup>3</sup> and Jean-Claude Tédénac<sup>1</sup>, Lattice stability and formation energies of intrinsic defects in  $\text{Mg}_2\text{Si}$  and  $\text{Mg}_2\text{Ge}$  via first-principles simulations. *Journal of Physics: Condensed Matter*, 2012. **25**(3): p. 035403.
58. Morris, R.G., R.D. Redin, and G.C. Danielson, Semiconducting Properties of  $\text{Mg}_2\text{Si}$  Single Crystals. *Physical Review*, 1958. **109**(6): p. 1909-1915.
59. Francesco Ricci, Wei Chen, Umut Aydemir, G. Jeffrey Snyder, Gian-Marco Rignanese, Anubhav Jain & Geoffroy Hautier, An ab initio electronic transport database for inorganic materials. *Scientific data*, 2017. **4**: p. 170085-170085.
60. Ong, K.P., D.J. Singh, and P. Wu, Analysis of the thermoelectric properties of n-type ZnO. *Physical Review B*, 2011. **83**(11): p. 115110.
61. Madsen, G.K.H. and D.J. Singh, BoltzTraP. A code for calculating bandstructure dependent quantities. *Computer Physics Communications*, 2006. **175**(1): p. 67-71.
62. Gonze, X., Interatomic Force Constants in Periodic Solids from Density Functional Perturbation Theory, in *Advances in Quantum Chemistry*, P.-O. Löwdin, Editor. 1998, Academic Press. p. 225-239.
63. Togo, A. and I. Tanaka, First-principles phonon calculations in materials science. *Scripta Materialia*, 2015. **108**: p. 1-5.
64. Chaput, L., Direct Solution to the Linearized Phonon Boltzmann Equation. *Physical review letters*, 2013. **110**: p. 265506.
65. Togo, A., L. Chaput, and I. Tanaka, Distributions of phonon lifetimes in Brillouin zones. *Physical Review B*, 2015. **91**(9): p. 094306.